Correlated lightning mapping array and radar observations of the initial stages of three sequentially triggered Florida lightning discharges

J. D. Hill,[1,2] J. Pilkey,[1] M. A. Uman,[1] D. M. Jordan,[1] W. Rison,[3] P. R. Krebhiel,[3] M. I Biggerstaff,[4] P. Hyland,[4] and R. Blakeslee[5]

Received 12 March 2013; revised 15 July 2013; accepted 16 July 2013.

[1] Correlated Lightning Mapping Array and vertical-scan radar images are presented for three rocket-and-wire triggered lightning flashes that occurred sequentially within 17 min in the presence of a decaying multicellular convective storm system over north-central Florida. The initial stage (IS) of each flash propagated generally vertically to the altitude of the 0°C melting level, about 5 km, and then subsequently propagated for many kilometers horizontally along the melting level contour. Radar images suggest that the propagation paths of the IS channels below and above the melting level were heavily influenced by precipitation gradients. Flash UF 11-24 exhibited a 12.6 km unbranched IS channel, the longest unbranched channel observed in the study by a factor of three. During flash UF 11-25 (119 ms following the cessation of the measured IS current at ground and prior to the first return stroke), a natural cloud-to-ground discharge, perhaps induced by the IS, initiated between 2.5 and 4 km altitude and struck ground 5 to 7 km from the launching facility. The IS of flash UF 11-26 propagated upward through a descending precipitation packet and apparently induced a naturally appearing bi-level intracloud discharge via an upward-negative leader that initiated within the IS breakdown region 3.5 km from the launching facility. The upward-negative leader propagated from 5.6 to 9.3 km altitude in a time of 11 ms. The electrical current measured at ground during the IS of flash UF 11-26 exhibited a 57 ms polarity reversal, transferring 19 C of positive charge to ground.

Citation: Hill, J. D., J. Pilkey, M. A. Uman, D. M. Jordan, W. Rison, P. R. Krebhiel, M. I Biggerstaff, P. Hyland, and R. Blakeslee (2013), Correlated lightning mapping array and radar observations of the initial stages of three sequentially triggered Florida lightning discharges, *J. Geophys. Res. Atmos.*, *118*, doi:10.1002/jgrd.50660.

1. Introduction

[2] *Hill et al.* [2012b] have characterized the initial stage (IS) geometry and the related channel-base current characteristics of nine rocket-and-wire triggered lightning flashes that were artificially initiated in the presence of convective thunderstorms in north-central Florida during summer 2011. The geometrical features of the IS processes of the nine flashes, such as the initiation altitudes of IS branches and channel propagation speeds, were determined using sources obtained with a local Lightning Mapping Array (LMA) [e.g., *Rison et al.*, 1999; *Krehbiel et al.*, 2000; *Thomas et al.*, 2004; *Edens et al.*, 2012]. *Edens et al.* [2012] used similar techniques to describe one triggered flash in New Mexico that exhibited much more extensive and lower altitude (relative to the triggering site) upward branching than that reported by *Hill et al.* [2012b]. Here, the work of *Hill et al.* [2012b] is extended via detailed examination of three of the nine triggered flashes, including the first correlations of the LMA-determined IS geometry with high-resolution, vertical-scan radar images. The three flashes under consideration, designated UF 11-24, UF 11-25, and UF 11-26, were triggered sequentially over a time period of about 17 min on 5 August 2011, during the decaying stage of a convective thunderstorm system.

2. Background and Experiment

[3] The process of triggering lightning from natural thunderstorms using the rocket-and-wire technique begins with the launching of a small rocket that elevates a grounded metallic triggering wire. At the International Center of Lightning Research and Testing (ICLRT) in north-central Florida, rockets are launched when the quasistatic electric field measured at ground surpasses a typical threshold of

[1]Department of Electrical and Computer Engineering, University of Florida, Gainesville, Florida, USA.
[2]Stinger Ghaffarian Technologies, Kennedy Space Center, Florida, USA.
[3]Electrical Engineering Department, Physics Department, New Mexico Institute of Mining and Technology, Socorro, New Mexico, USA.
[4]School of Meteorology, University of Oklahoma, Norman, Oklahoma, USA.
[5]NASA Marshall Space Flight Center, Huntsville, Alabama, USA.

Corresponding author: J. D. Hill, Department of Electrical and Computer Engineering, University of Florida, PO Box 116200, 311 Larsen Hall, Gainesville, FL 32611, USA. (jonathan.d.hill@nasa.gov)

2169-897X/13/10.1002/jgrd.50660

Table 1. Distance and Azimuth Angle From the ICLRT Launching Facility to Each LMA Station

Measurement	Distance From Launcher (m)	Azimuth (°)
LMA site 1	461	64
LMA site 2	2988	277
LMA site 3	2773	134
LMA site 4	5396	188
LMA site 5	7701	357
LMA site 6	5535	296
LMA site 7	9608	252

about +5 kV/m (physics sign convention—electric field vector pointing upward, that is, with predominantly negative cloud charge overhead). About half of such launches result in the initiation of an upward-propagating positively charged leader (UPL) from the ascending wire top, subsequently vaporizing the triggering wire, and frequently, after that, resulting in one or more leader/return stroke sequences. A typical triggering process is now described. As the rocket ascends at a speed of the order of 150 m/s, transient electrical breakdown events termed "precursor current pulses" (or just "precursors") occur at the wire tip [e.g., *Lalande et al*., 1998; *Willett et al*., 1999; *Biagi et al*., 2009, 2012]. The precursors are electrical sparks at the top of the wire that fail to evolve into a sustained UPL. When the wire top reaches a typical height of 200–400 m, a UPL is launched from the wire top and subsequently propagates towards the negative cloud charge at a speed of the order of 10^5 m/s. The triggering wire typically explodes when the UPL reaches an altitude of 1–2 km, usually 5–10 ms after its initiation, during which time the wire extends upward only a few meters. The current measured at the triggered lightning channel base rises to a typical amplitude of about 100 A as the UPL ascends, often dropping abruptly to a level at or near zero during the triggering wire explosion, and then resuming a background level of about 100 A that persists for typically several hundred milliseconds. This long-duration current, which often transfers tens of coulombs of negative charge to ground and can have superimposed current pulses with amplitudes of the order of a thousand amperes, is referred to as the "initial continuous current" or ICC. The precursor current pulses, the UPL, and the ICC together compose the initial stage (IS) of the triggered lightning flash. There is no clear demarcation between the UPL and ICC. Hereafter, the term "UPL" is used only to refer to the upward-propagating leader channel prior to channel branching, while the term "UPL/ICC" refers to the time period extending from the initiation of the UPL through the end of the IS period. Often, after the cessation of the IS, dart leader/return stroke sequences, very similar to subsequent strokes in natural lightning, follow the path of the IS channel between negative cloud charge and ground. Triggered lightning discharges usually lower negative charge during both the IS and the dart leader/return stroke sequences. The negative charge lowered to ground may originate in the primary negative charge region of the cloud located at an altitude above the 0°C level, the 0°C level being at 4–5 km in north central Florida [e.g., *Harris et al*., 2000; *Hansen et al*., 2010], with an estimated lower and upper bound for the primary negative charge region in developing and mature stage storms of roughly 6 and 8 km corresponding to temperatures of −10°C and −20°C, respectively [e.g., *Krehbiel*, 1986; *Gremillion and Orville*, 1999]. The same negative charge region is thought to be the primary source of natural negative lightning to ground. Occasionally, positive charge is transferred to ground as part of the overall triggered flash [e.g., *Jerauld et al*., 2004; *Yoshida et al*., 2012], as discussed further in section 3.3 (flash UF 11-26).

[4] For triggered flashes UF 11-24, UF 11-25, and UF 11-26, the IS channels are mapped in three dimensions via the time-of-arrival (TOA) locations of VHF sources associated with the leader tip breakdown as obtained from a local seven-station LMA. The leader tip breakdown involves a radiating current source that extends positive charge to form a new channel section, with the resultant negative charge moving back along the extending channel. Each LMA station records the time of the peak VHF power (66–72 MHz) received in consecutive 80 μs windows. The acquisition windows are synchronized at the different geographic station locations via GPS receivers. The distances and azimuth angles of the seven LMA stations relative to the launching facility at the ICLRT are given in Table 1 and are shown graphically in Figures 5, 10, and 15. The 3-D LMA source locations and emission times are calculated using the nonlinear least squares optimization technique described in *Thomas et al*. [2004]. Unless otherwise noted, for all LMA data presented, source locations are plotted only to the time of the end of the IS period, this time being determined from the correlated channel-base current measurements. All LMA plots including lateral coordinates have positive axis labels corresponding to increasing distance in the northerly and easterly directions. For UF 11-24, UF 11-25, and UF 11-26, only six LMA stations were operational. LMA data used in the analyses presented are thus for five- or six-station solutions with reduced chi-square values less than 4, when corrected for the 30 ns actual timing errors of the network. The current during the IS was measured at the lightning channel base on three different sensitivity scales with a 0.001 Ω T&M Research R-7000-10 current-viewing resistor. The current measurements are designated high, low, and very low and have respective sensitivities of about 63 kA, 6.3 kA, and 202 A per digitizer volt, with a full-scale measurement corresponding to 1 V output. The normal component of the time-varying electric field was sensed by an inverted flat plate capacitive antenna located 184 m from the launching facility. The antenna had sensitivity of about 197 kV/m per digitizer volt (full-scale output of 1 V) and a decay time constant of 8 s. Channel-base current and electric field waveforms were digitized with 12-bit resolution at 10 MS/s on Yokogawa DL750 digital storage oscilloscopes whose anti-aliasing filter limited the upper frequency response to 3 MHz.

[5] The University of Oklahoma C-band (5.589 GHz) dual polarimetric SMART radar [e.g., *Biggerstaff et al*., 2005] was located at the Keystone Airpark, 11.6 km to the south of the ICLRT. When thunderstorm conditions were present, the radar operated in range-height indicator (RHI) mode, acquiring 5° azimuthal sector scans above the triggering facility every 90 s. The vertical-scan radar images were used to determine the hydrometeor structure in the vicinity of the triggered lightning discharges and to determine the altitude of the 0°C melting level. The altitude of the 0°C level was also available from atmospheric soundings taken at the Jacksonville, FL National Weather Service (NWS) station. Additional radar information was available from the S-band (2.7–3.0 GHz) NWS Weather Surveillance Radar-1988

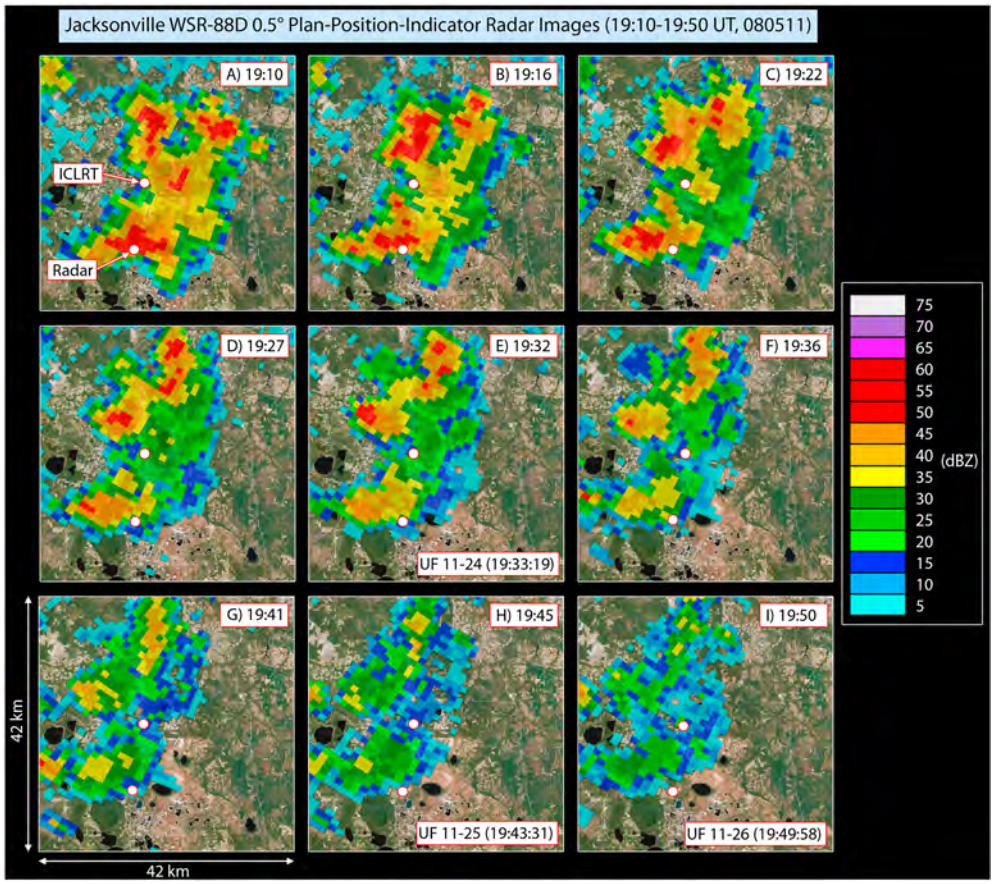

Figure 1. Nine sequential 0.5° plan position indicator (PPI) scans over the region surrounding the ICLRT obtained by the Jacksonville WSR-88D S-band radar, located 68 km to the northeast. The radar images show the decaying stages of multiple convective cells to the north and south of the ICLRT. The locations of the ICLRT and the SMART radar are annotated. Each radar image is 42 × 42 km.

Doppler (WSR-88D) [e.g., *Crum and Alberty*, 1993] located near Jacksonville, FL, 68 km to the north-northeast of the ICLRT, allowing the documentation of the larger horizontal-scale structure of the cloud systems. At the range of the ICLRT from the Jacksonville radar site, the centers of the 0.5° and 2.4° elevation radar beams from the WSR-88D were at altitudes of about 600 m and 2.9 km, respectively.

3. Data: Three Sequential-Triggered Lightning Flashes on 5 August 2011

[6] At about 17:20 (UT) on 5 August 2011, convection initiated a distance of 35 to 40 km southeast of the ICLRT, well inland of the sea-breeze circulation that was located near the Florida east coast, about 40 km farther away. Within 1 h, the cloud system grew to form a north–south oriented quasi-linear convective band that was roughly 35 km in length. In the deepest part of the cluster, radar echo tops from the Jacksonville WSR-88D extended to about 14 km in altitude. The convective band propagated westward at a speed of 5.5 m/s, arriving just east of the ICLRT at 19:00 (UT). Shortly afterward, the central part of the system started to dissipate while new convective cells continued to form to the north-northwest and south-southwest of the ICLRT. The new cells also exhibited echo tops of about 14 km. The Jacksonville NWS sounding at 12:00 (UT) reported the 0° C level at an altitude of about 4.9 km. Nine consecutive PPI radar images acquired at a 0.5° elevation angle (600 m over the ICLRT) by the Jacksonville WSR-88D from 19:10 to 19:50 (UT) are shown in Figure 1. An additional nine consecutive PPI images acquired at a 2.4° elevation angle (2.9 km over the ICLRT) are shown for the same time period in Figure 2. Flashes UF 11-24, UF 11-25, and UF 11-26 were triggered in the 17 min between 19:33:19 (UT) and 19:49:58 (UT) and are annotated in Figures 1 and 2. During that 17 min, there were five natural cloud-to-ground flashes within 10 km of the ICLRT according to the National Lightning Detection Network, whereas during 15 min intervals 15, 30, and 45 min earlier, there were 11, 19, and 29 natural cloud-to-ground flashes, respectively, showing a decaying storm in accord with the radar images of Figures 1 and 2. Correlated observations of the LMA source locations, measured channel-base currents, and SMART radar RHI images of the IS processes of flashes UF 11-24, UF 11-25, and UF 11-26 are discussed below. Still photographs of the bottom 275 m of the three triggered lightning discharges under study are shown in Figure 3. The photographs were taken looking due east from a western location at the ICLRT, and each is a 5 s time exposure.

3.1. Flash UF 11-24

[7] Flash UF 11-24 was triggered at 19:33:19 (UT) on 5 August 2011 with a quasistatic electric field at ground of

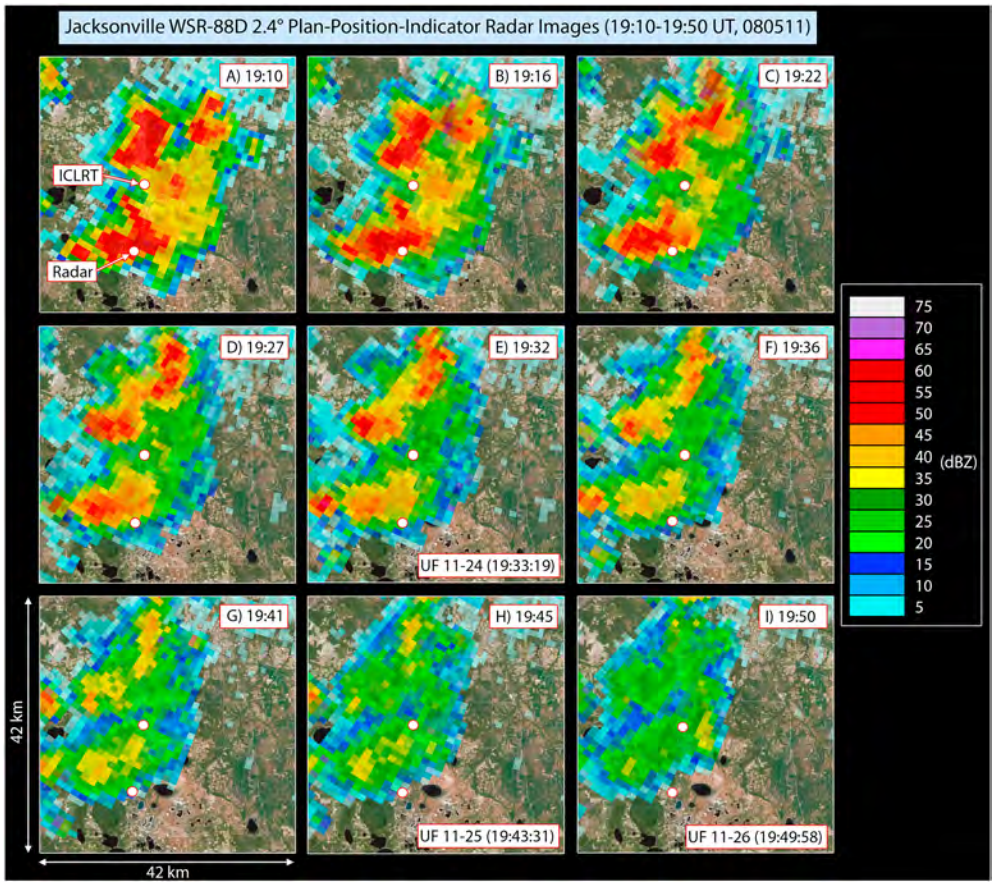

Figure 2. Nine sequential 2.4° plan position indicator (PPI) scans over the region surrounding the ICLRT obtained by the Jacksonville WSR-88D S-band radar, located 68 km to the northeast. The radar images show the decaying stages of multiple convective cells to the north and south of the ICLRT. The locations of the ICLRT and the SMART radar are annotated. Each radar image is 42 × 42 km.

about +5.5 kV/m. The flash contained an IS process followed by one dart leader/return stroke sequence, the return stroke having a peak current of 33 kA, the largest peak current recorded during summer 2011. The UPL/ICC had a duration of 425 ms and transferred 46 C of negative charge to ground. A 3-D view of the LMA source locations during the IS period of flash UF 11-24 is shown in Figure 4. Four projection views of the LMA source locations for flash UF 11-24 are shown in Figure 5. In both Figures 4 and 5, the LMA source locations associated with precursor current pulses during the triggering wire ascent are colored in bright green irrespective of emission time, while subsequent LMA sources obtained during the UPL/ICC are color coded in 50 ms bins according to the respective keys at right. The 0°C level from the Jacksonville NWS sounding (4.9 km) is annotated in all plots that show LMA source altitude coordinates. The LMA located a significant number of precursor current pulses (Figure 5c) within the 400 ms prior to the initiation of the UPL. The UPL initiated at about 0.95 s in Figure 5c at an altitude of about 185 m (Figure 3a) and is clearly differentiated from the preceding precursor pulses by the abrupt change in propagation speed. The triggering wire exploded about 4.6 ms after the initiation of the sustained UPL when the UPL was at an altitude of about 1.3 km. The UPL propagated generally vertically to an altitude of about 4.7 km with no detected upward branching (Figure 5b), then turned 90° to the north and propagated generally horizontally for about 6 km. Here, the IS channel branched with one channel propagating to the northeast and the other to the west (Figures 5a and 5d). Not accounting for channel tortuosity, the northeast IS channel progressed for about 5 km, branching once more, at an average altitude of about 4.7 km. The western IS channel also branched once more over a propagation distance of about 4 km as it ascended to an altitude of about 6.7 km (Figure 5a), after which the LMA sources became more diffuse as the IS channel exhibited significant horizontal branching to the north and west (Figure 5d). The two primary regions of electrical breakdown from the northeast and western IS branches were eventually separated by as much as 14 km laterally and by about 2 km in altitude. The initial IS channel prior to channel branching had a total length, accounting for large-scale channel tortuosity, of about 12.6 km, the longest observed unbranched initial UPL channel during summer 2011 by more than a factor of three. The LMA source locations were used to estimate the lengths and average propagation speeds of the initial UPL and the four clearly defined IS branches, which are labeled in Figures 5b and 5d in order of increasing initiation time. A discussion of the procedures involved in these calculations is given in *Hill et al*. [2012b]. The initial UPL of flash UF 11-24 traversed a 12.6 km distance with an average speed of about 8.4×10^4 m/s. The two western IS

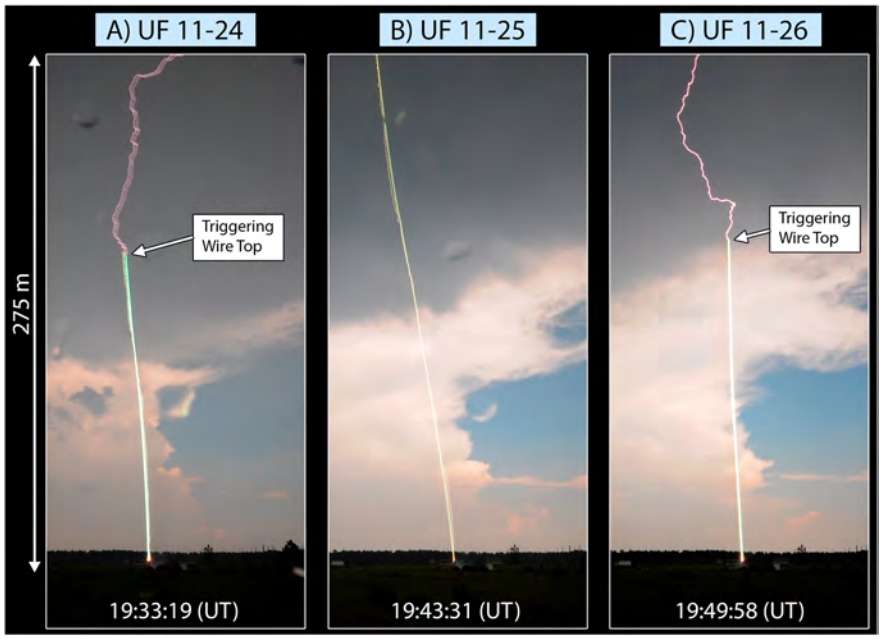

Figure 3. Time-exposed still images of flashes (a) UF 11-24, (b) UF 11-25, and (c) UF 11-26. The top of the images correspond to an altitude 275 m above the launching facility. The triggering wire height was 185 m for flash UF 11-24, 455 m for flash UF 11-25 (above the photograph frame), and 177 m for flash UF 11-26.

channels (branches 1 and 3 in Figure 5) propagated for distances of 5.2 km and 6.2 km at average speeds of 1.7×10^4 m/s and 1.9×10^4 m/s, respectively. The northeast IS channels (branches 2 and 4 in Figure 5) propagated for total distances of 6.5 and 7.2 km at speeds of 2.1×10^4 m/s and 3.3×10^4 m/s, respectively.

[8] In Figure 6, the altitude projection of the LMA source locations is overlaid on a 910 ms record of the channel-base current. The channel-base current is plotted to the end of the IS period. The low channel-base current measurement (refer to section 2) is shown because the more sensitive measurement (very low) saturated at the time of the 2.4 kA ICC

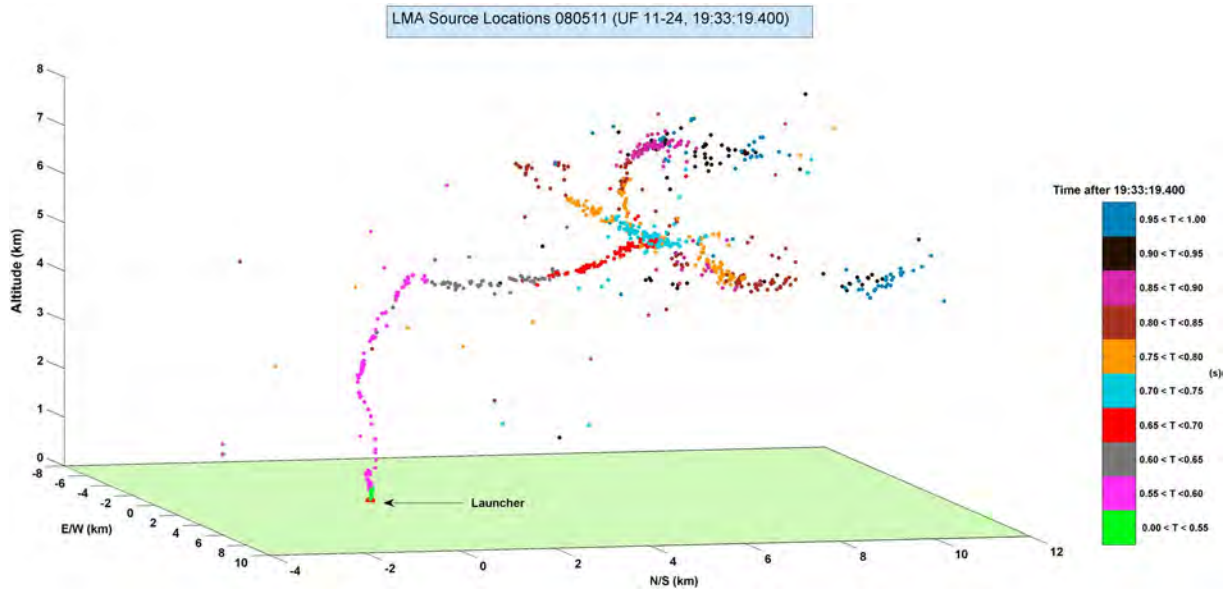

Figure 4. Three-dimensional plot of the LMA source locations for the IS period of flash UF 11-24 on 5 August 2011. The sources span a total of 1 s beginning at 19:33:19.400 (UT). All LMA sources corresponding to precursor current pulses are colored in bright green and occupy the initial 550 ms of the displayed time window. LMA sources during the remainder of the IS process are color coded according to the key at right in 50 ms bins.

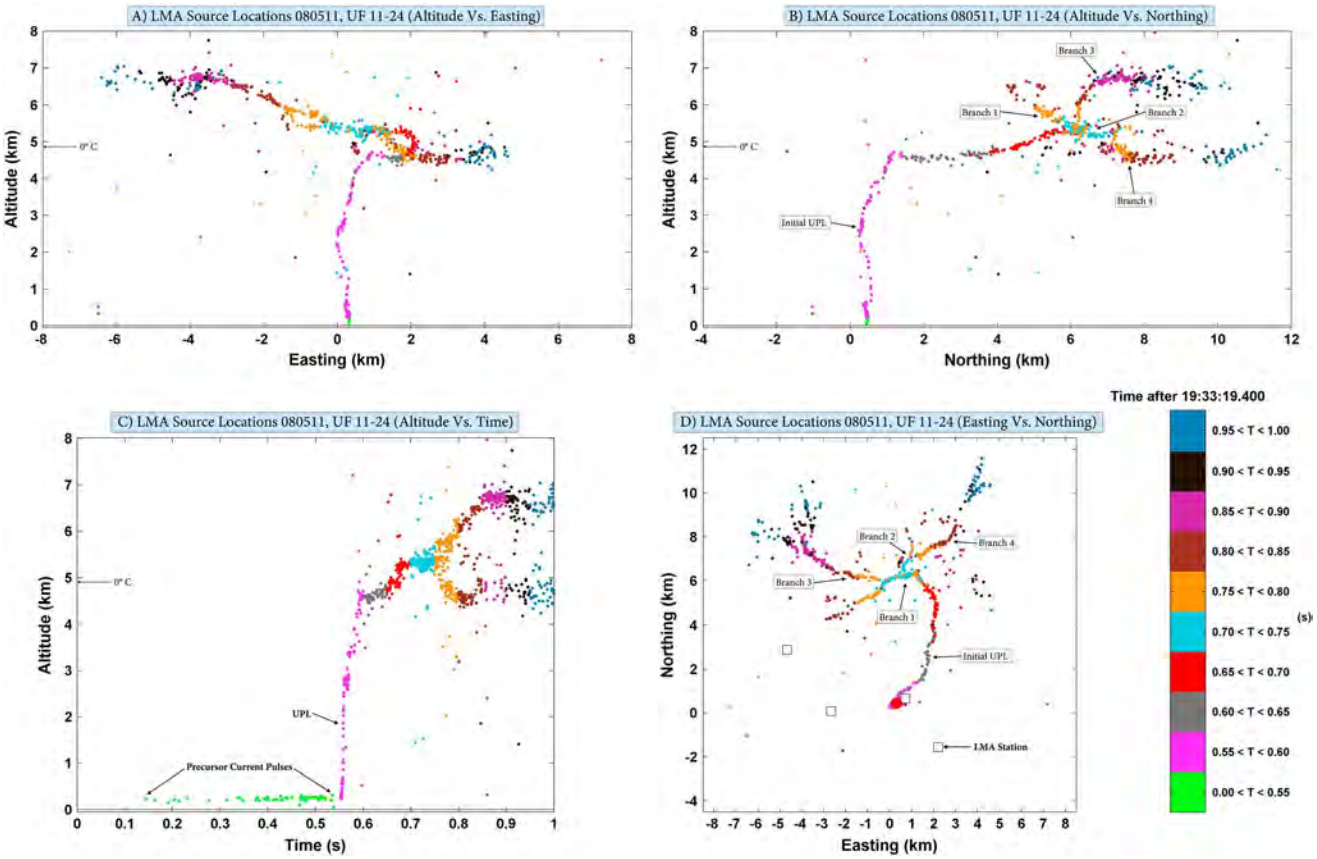

Figure 5. Four projection views of the LMA source locations during the IS period of flash UF 11-24 on 5 August 2011. (a) An easting versus altitude plot (view looking due north), (b) a northing versus altitude plot (view looking due west), (c) an altitude versus time plot, and (d) an easting versus northing plot (plan view, launching facility annotated by large red circle at about (0,0)). The sources span 1 s in time beginning at 19:33:19.400 (UT) and are color coded according to the convention of Figure 4. The initial UPL and four IS branches are labeled with increasing initiation time. The initiation altitudes of the four IS branches were 5.4, 5.4, 5.4, and 5.2 km, respectively.

pulse that occurs at about 490 ms in Figure 6. The initiation times of the four clearly defined IS branches are annotated on the channel-base current waveform with red diamonds. A 250 ms segment of the very low channel-base current waveform around the times of the IS branches (corresponding to the time region enclosed by the orange dotted lines) is expanded in the inset of Figure 6. The branches initiated at current amplitudes ranging from 90–125 A, and all occurred following the initial current variation (ICV) associated with the explosion of the triggering wire [e.g., *Wang et al.*, 1999; *Rakov et al.*, 2003; *Olsen et al.*, 2006]. The ICV, as noted earlier, occurred 4.6 ms after the initiation of the sustained UPL but is not clearly evident in Figure 6. The IS branch initiation current amplitudes were determined from the very low current waveform with ampere-level resolution. Branches 1 and 2 occurred nearly coincident with the peak of an increase of current that elevated the channel-base current from 50 to 95 A (after which the current decreased) while the final two IS branches were not associated with any prominent waveform feature.

[9] SMART radar RHI scans of equivalent radar reflectivity factor (dBZ) and differential radar reflectivity factor (Z_{DR}) collected at the time of flash UF 11-24 are shown in Figure 7. The data were first threshold on correlation coefficient less than 0.7 to remove noise and then smoothed using a 3×3 median filter to remove small-scale fluctuations. LMA sources located within 10 km of the radar sweep plane, the center of which is pointed approximately north, are projected into the cross section and shown as black (red) crosses if the source locations were east (west) of the RHI plane. The melting layer is clearly marked by the rapid decrease in Z_{DR} and dBZ above 4.5 km altitude, in good agreement with the 12:00 (UT) NWS sounding taken at Jacksonville. High values of Z_{DR} indicate oblate hydrometeors with high-dielectric constant, such as large raindrops and melting snow, while low values of Z_{DR} indicate spherical (smaller) raindrops or dry ice particles with low dielectric constant, like frozen snow and ice crystals [e.g., *Zrnic and Ryzhkov*, 1999]. Radar reflectivity is the sum of the sixth power water-equivalent diameter of the hydrometeors within a unit volume of air. Hence, radar reflectivity provides information on both particles size and number concentration while Z_{DR} provides information on particle shape, size, and phase. According to the radar reflectivity (Figure 7a), the rocket was launched within light precipitation at ground level (also see the still photograph in Figure 3a). The IS propagated upward, with little deviation from the vertical, along gradients in particle size (Figure 7b) and through a dissipating convective region just above the ICLRT (Figure 7a). Near-zero Z_{DR} values with reflectivities

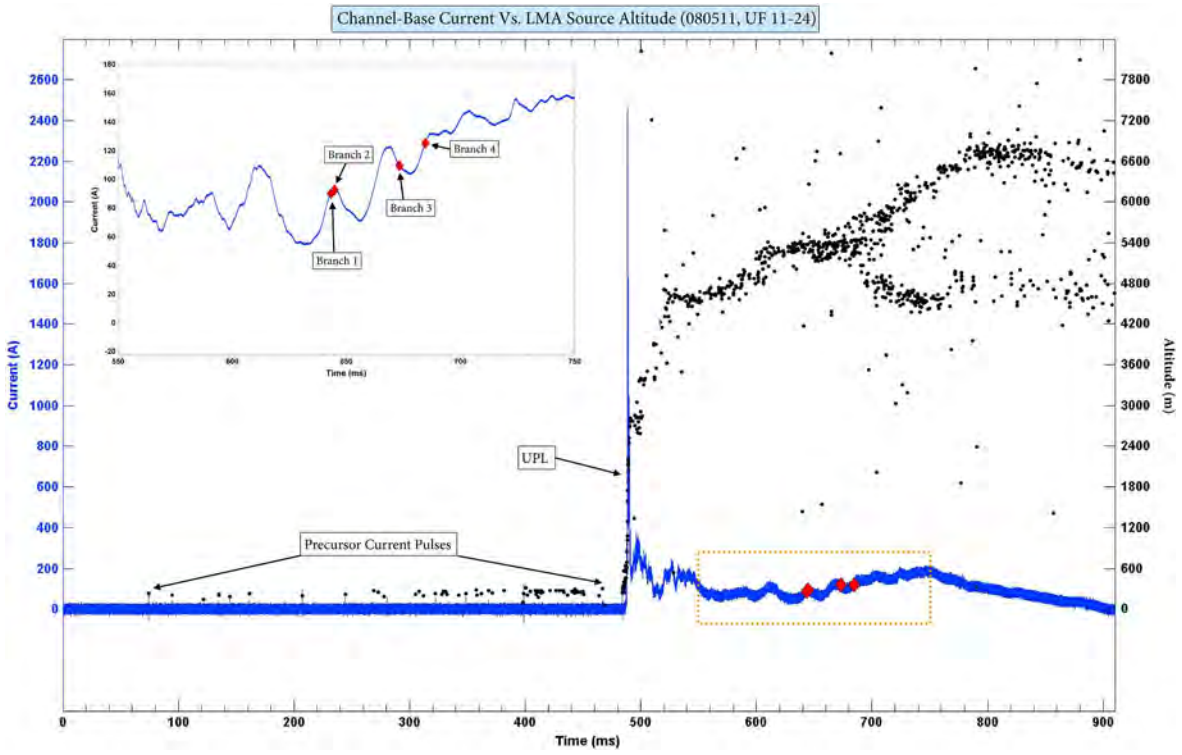

Figure 6. LMA source altitude locations (black points) for the IS period of flash UF 11-24 on 5 August 2011 overlaid on a 910 ms window of the low channel-base current measurement. The final 485 ms of the wire ascent and the full 425 ms duration of the UPL/ICC are shown. Sources are annotated corresponding to precursor current pulses. Red diamonds superimposed on the current waveform indicate the times of the four IS branches. The inset at upper left shows a 200 ms window of the very low channel-base current waveform around the times of the four IS branches labeled in Figure 5.

around 30 dBZ indicate the dissipating convection consisted of small rain drops. At the top of the Z_{DR}-indicated melting layer, the IS turned abruptly horizontal and followed the top of the melting layer for about 6 km prior to exhibiting the branched structure described previously.

[10] The initial branch in the flash occurred at 17 km range from the radar near the bottom of an enhanced reflectivity column that extended 4 km above the top of the melting layer. This area was also coincident with a transition from an elevated positive Z_{DR} region to an area of negative Z_{DR} along the IS path. Thus, the IS branch occurred in an area in which the hydrometeors dominating the radar backscatter switched from small water-coated particles to small frozen particles. The tops of positive Z_{DR} columns above the melting layer are often preferred regions of initial electric field breakdown in naturally occurring in-cloud and cloud-to-ground flashes [e.g., *Lund et al*., 2009]. Aircraft penetrations into other Florida thunderstorms found that the strongest electric fields occurred within the transition regions between updrafts and downdrafts where mixed phase particles were most abundant [e.g., *French et al*., 1996]. Hence, the transition region between water-coated and frozen particles observed here may be an area of enhanced electric fields. The northeast IS branch propagated for several more kilometers along the top of the melting layer before terminating within a mature stage convective cell to the north-northeast of the ICLRT. It should be noted that the LMA sources once again propagated along the top of the positive Z_{DR} region, even as it dipped to lower altitudes in the mature cell. The western IS branch propagated towards a separate cell outside the plane of the RHI scan.

[11] The distribution of LMA source altitudes for the IS of flash UF 11-24 is shown in Figure 8, reproduced from *Hill et al*. [2012b]. The distribution includes 909 sources and the histogram is smoothed with bin width of 30 points. The large peak at altitudes less than 1 km is due to the precursor current pulses and the initial UPL points. The peak between 4 and 5 km is due to the horizontally propagating UPL following the 90° northerly turn when the discharge reached the altitude of the 0°C level (Figure 5b). The peak between 5 and 6 km is due to the breakdown region initiated by the northeast IS branches, and the higher-altitude peak between 6 and 7 km is due to the breakdown region initiated by the western IS branches (Figure 5a).

3.2. Flash UF 11-25

[12] Flash UF 11-25 was triggered at 19:43:30 (UT), about 10 min after UF 11-24. The quasistatic electric field measured at the ground at the time of the rocket launch was +4.6 kV/m. Flash UF 11-25, like UF 11-24, contained an IS process and one dart leader/return stroke sequence. The return stroke peak current was 12 kA, typical for triggered lightning strokes. The UPL/ICC had duration of 404 ms and transferred 28 C of negative charge to ground. A 3-D plot of the LMA source locations obtained during flash UF 11-25 is shown in Figure 9, and four projections views of the LMA sources are shown in Figure 10. The LMA sources span 4 s,

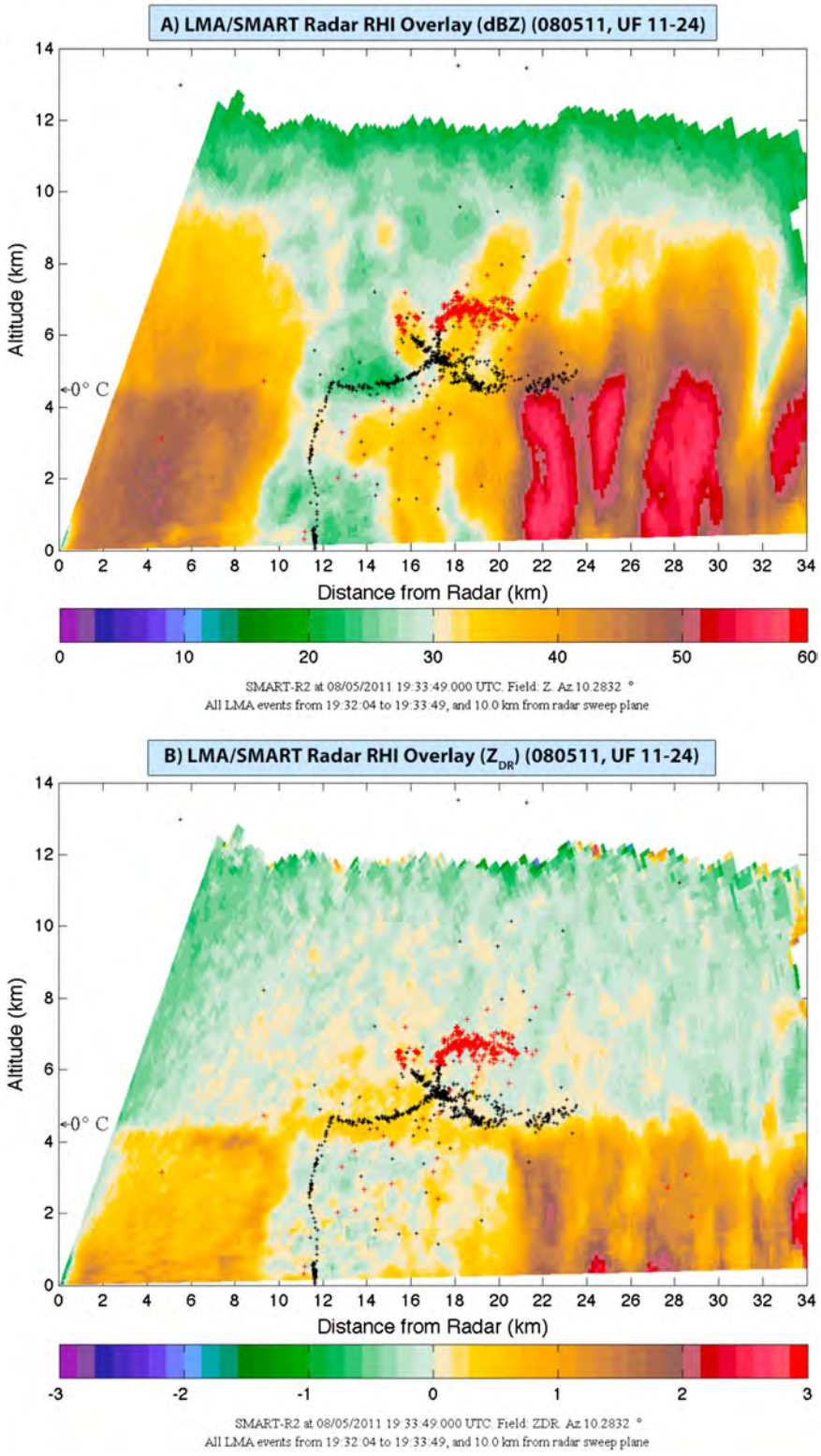

Figure 7. Modified RHI scans taken by the SMART radar at the time of flash UF 11-24 on 5 August 2011. (a) Filtered radar reflectivity (dBZ) with northing projection of LMA IS source locations overlaid. (b) Filtered and bias-corrected differential radar reflectivity factor (dB) with northing projection of LMA IS source locations overlaid. Projected LMA sources within 10 km of the RHI plane are plotted as black (red) crosses for source locations to the east (west) of the plane.

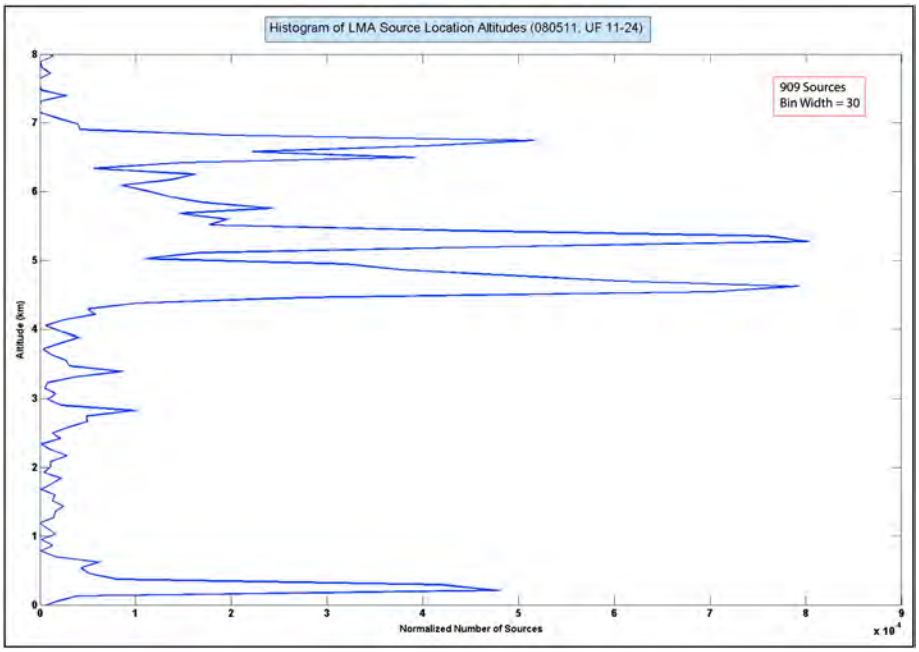

Figure 8. Histogram (bin size equal to 30 sources) of the altitude distribution of LMA IS sources of flash UF 11-24 on 5 August 2011.

with sources associated with precursor current pulses colored in bright green and sources corresponding to the UPL/ICC color coded according to the key at right in 50 ms bins. Flash UF 11-25 exhibited a large number of precursor current pulses during the 4.4 s duration of the wire ascent (Figure 10c) prior to the initiation of the sustained UPL at an altitude of about 455 m. The LMA recorded source locations for more than 50 precursor current pulses in a time of about 3 s. The UPL initiated at about 19:43:34.377 (UT), or about 3.6 s in the altitude versus time projection of Figure 10c and, as for UF 11-24, is distinguished from the preceding precursor pulses by the abrupt change in propagation speed. Flash UF 11-25 had a total of six clearly defined IS branches following the initial UPL. The IS branches are labeled in Figures 10b and 10d in order of increasing initiation time.

[13] The initial UPL of flash UF 11-25 ascended to an altitude of about 750 m at an average speed of 7.9×10^4 m/s. Branch 1 (Figure 10b) initiated at 750 m altitude and propagated

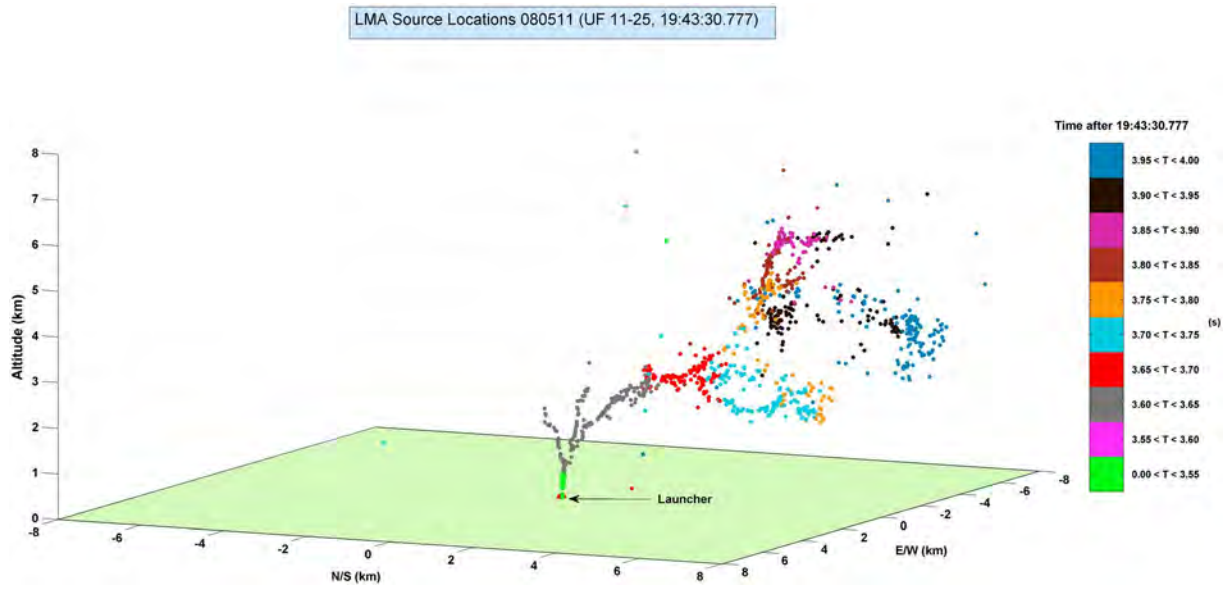

Figure 9. Three-dimensional plot of the LMA IS source locations for flash UF 11-25 on 5 August 2011. The sources span a total of 4 s beginning at 19:43:30.777 (UT). All LMA sources corresponding to precursor current pulses are colored in bright green and occupy the initial 3.55 s of the displayed time window. LMA sources during the remainder of the IS process are color coded according to the key at right in 50 ms bins.

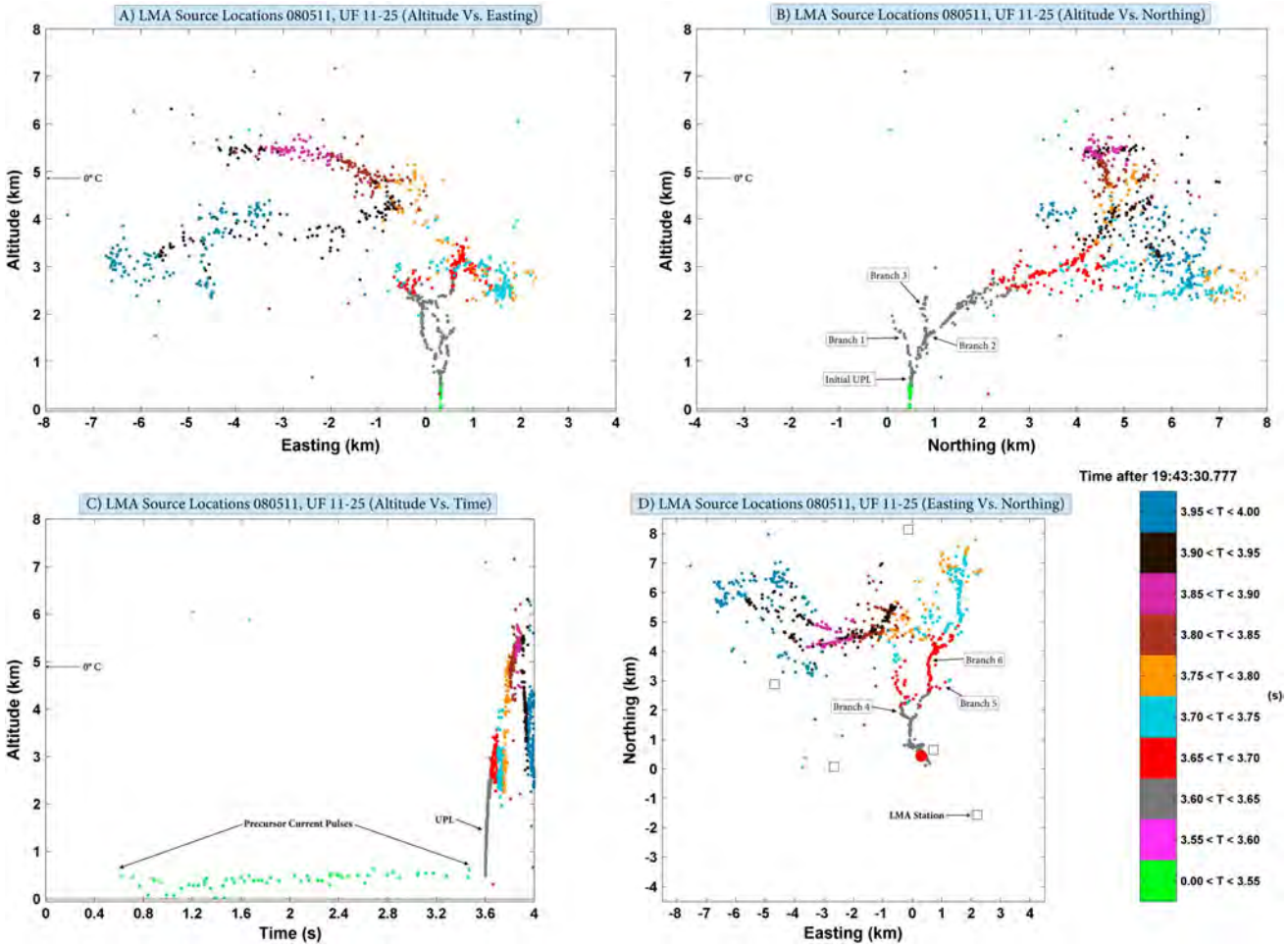

Figure 10. Four projection views of the LMA source locations for the IS period of flash UF 11-25 on 5 August 2011. (a) An easting versus altitude plot (view looking due north), (b) a northing versus altitude plot (view looking due west), (c) an altitude versus time plot, and (d) an easting versus northing plot (plan view, launching facility annotated by large red circle). The sources span 4 s in time beginning at 19:43:30.777 (UT) and are color coded according to the convention of Figure 9. The initial UPL and six IS branches are labeled with increasing initiation time. The initiation altitudes of the six IS branches were 750, 750, 1.2, 2.3, 2.6, and 2.6 km.

upward and in a southeasterly direction for about 1.3 km at an average speed of 7.9×10^4 m/s, eventually stopping at an altitude of about 2 km. Branch 2 (Figure 10b) initiated nearly simultaneously with branch 1 at an altitude of about 750 m and propagated in a northerly and upward direction for about 3.3 km at a speed of 7.7×10^4 m/s. Branch 3 (Figure 10b) split from branch 2 about 4 ms after the initiation of branch 2. Branch 3 traveled at an average speed of 7.0×10^4 m/s in an upward and slightly southwesterly direction for about 1.7 km before apparently halting at an altitude of about 2.3 km. Branch 4 (Figure 10d) similarly split from branch 2 at an altitude of about 2.3 km (25 ms after the initiation of branch 2) and subsequently propagated for about 700 m to the northwest at an average speed of 3.5×10^4 m/s before stopping at an altitude of 2.5 km. Branch 2 finally split into branches 5 and 6 at an altitude of about 2.6 km. Branch 5 (Figure 10d) traveled to the east-northeast for about 900 m at a speed of 2.8×10^4 m/s and branch 6 (Figure 10d) traveled to the north-northeast for about 1.9 km at a speed of 4.3×10^4 m/s. Branch 6 initiated extensive horizontally oriented branching that eventually led to the widespread area of positive breakdown evident in Figures 10a, 10b, and 10d located between 3 and 6 km altitude.

[14] The altitude projection of the LMA source locations (Figure 10c) is overlaid on a 590 ms waveform of the measured channel-base current in Figure 11. The current waveform plotted is from the very low current measurement (unlike the IS of UF 11-24, there were no large current pulses that saturated the vertical scale of the measurement). The initiation times of the six IS branches described above are annotated on the current waveform with red diamonds. A 70 ms segment of the channel-base current waveform around the time of the IS branches is expanded in the inset of Figure 11 at upper left. Branches 1–3 initiated within 7 ms of the beginning of the UPL. There was no clearly defined ICV in the channel-base current waveform, but given the average time duration between the UPL and the ICV of 7.5 ms (measured for 37 triggered flashes at the ICLRT between 2009 and 2011), it is likely that at least branches 1 and 2, which both initiated within 3 ms of the beginning of the UPL, occurred prior to the wire explosion. The six IS branches initiated with channel-base

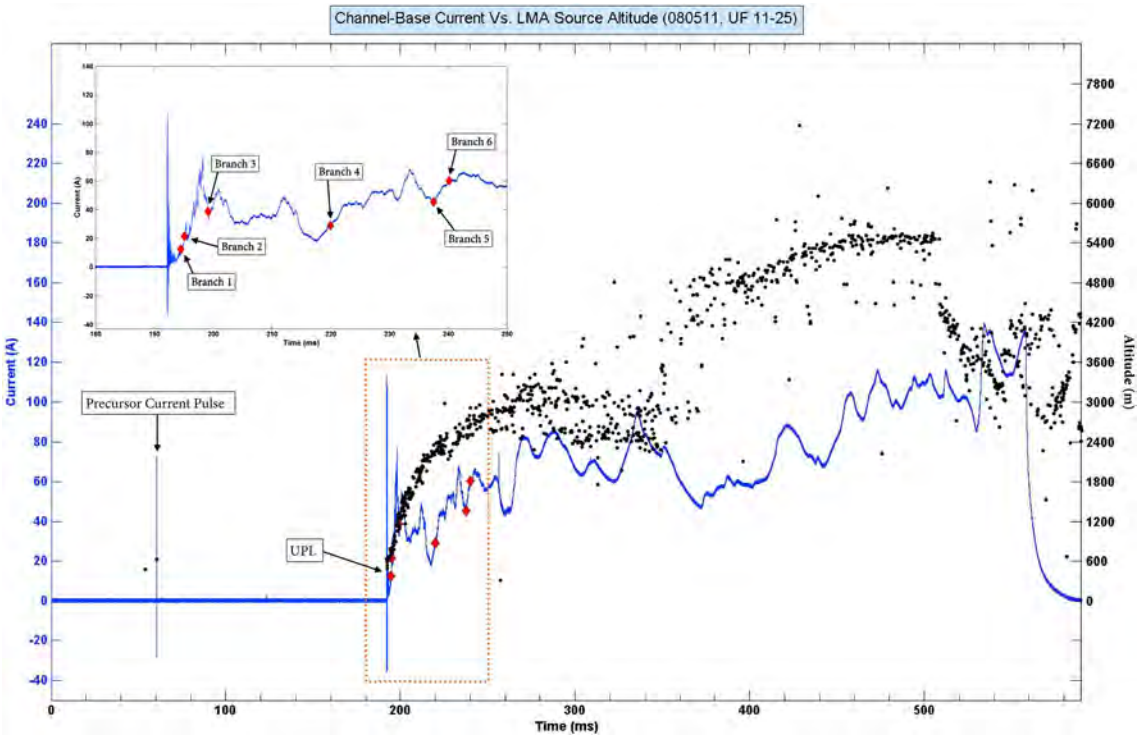

Figure 11. LMA source altitude locations (black points) for the IS period of flash UF 11-25 on 5 August 2011 overlaid on a 590 ms window of the low channel-base current measurement. The final 186 ms of the wire ascent and the full 404 ms duration of the UPL/ICC are shown. Sources are annotated corresponding to precursor current pulses. Red diamonds superimposed on the current waveform indicate the times of the six IS branches. The inset at upper left shows a 70 ms window of the very low channel-base current waveform around the times of the six IS branches labeled in Figure 10.

current amplitudes ranging from 12–60 A. None of the six IS branches was associated with prominent channel-base current waveform characteristics.

[15] SMART radar RHI scans of dBZ and Z_{DR} at the time of flash 11-25 are shown in Figure 12. The projection of the LMA source locations (Figure 10b) is overlaid on both radar images with the same source-coloring convention described for flash UF 11-24 (Figure 7). The peak radar reflectivity decreased in both of the cells to the north-northeast and south-southwest of the ICLRT (Figure 12a), consistent with the PPI observations of decaying convective cells from the Jacksonville WSR-88D shown in Figures 1g and 2g. In addition, the reflectivity immediately over the launching facility had decreased to less than 20 dBZ with Z_{DR} values near zero, indicative of light drizzle. There were clear sky conditions to the east (Figure 3b). The initial UPL and branches 1–3 propagated upward through very light precipitation. Branches 1 and 3 both halted slightly above 2 km altitude near the base of a shallow descending precipitation packet (PP) between 2 and 3 km in altitude and 11–15 km in horizontal range from the radar. Branches 2, 5, and 6 propagated in northerly directions generally within the plane of the radar RHI scan eventually tapping into the middle portion of an area of higher reflectivity centered at about 18 km from the radar (5.4 km from the launch facility) and about 3 km in altitude. The radar reflectivity of this feature exceeded 35 dBZ. The Z_{DR} values changed from negative values aloft to positive values below, indicating that the descending precipitation was likely a mixture of graupel and rain aloft with pure rain below. The end of branch 6 roughly followed the interface between the positive and negative Z_{DR} regimes. *Carey and Rutledge* [1996] noted that the cloud-to-ground lightning flash rate was well correlated with the mass of large graupel and small hail below the melting layer of a thunderstorm they observed over Colorado. Apparently, descending precipitation can be associated with significant charge, which may explain why much of the IS of flash UF 11-25 was found below the melting level.

[16] A portion of the IS did extend vertically to the top of the melting layer and just above. This vertical extension of the IS traversed the weak reflectivity area (around 15 km range from the radar) between the two enhanced precipitation regions. Once the IS reached the top of the melting layer, part of it turned horizontal and propagated along the top of the Z_{DR}-indicated melting layer, following a similar propagation path to flash UF 11-24 (Figure 10a). Additional LMA sources were found above 5 km and tended to be near transitions between negative and positive Z_{DR} values in the presumably negative charge region of the cloud system.

[17] Some of the western IS branching occurred out of the plane of the radar RHI scan (LMA sources shown in red in Figure 12). A second region of positive electrical breakdown between 2.5 and 4 km altitude later occurred to the northwest of the launching facility below the aforementioned discharge that propagated horizontally in the vicinity of the 0°C level (dark blue sources in Figure 10a). Of particular significance, a natural negative cloud-to-ground discharge initiated in the area of the lower altitude western LMA sources between 2.5 and 4 km altitude about 119 ms after the end of the IS

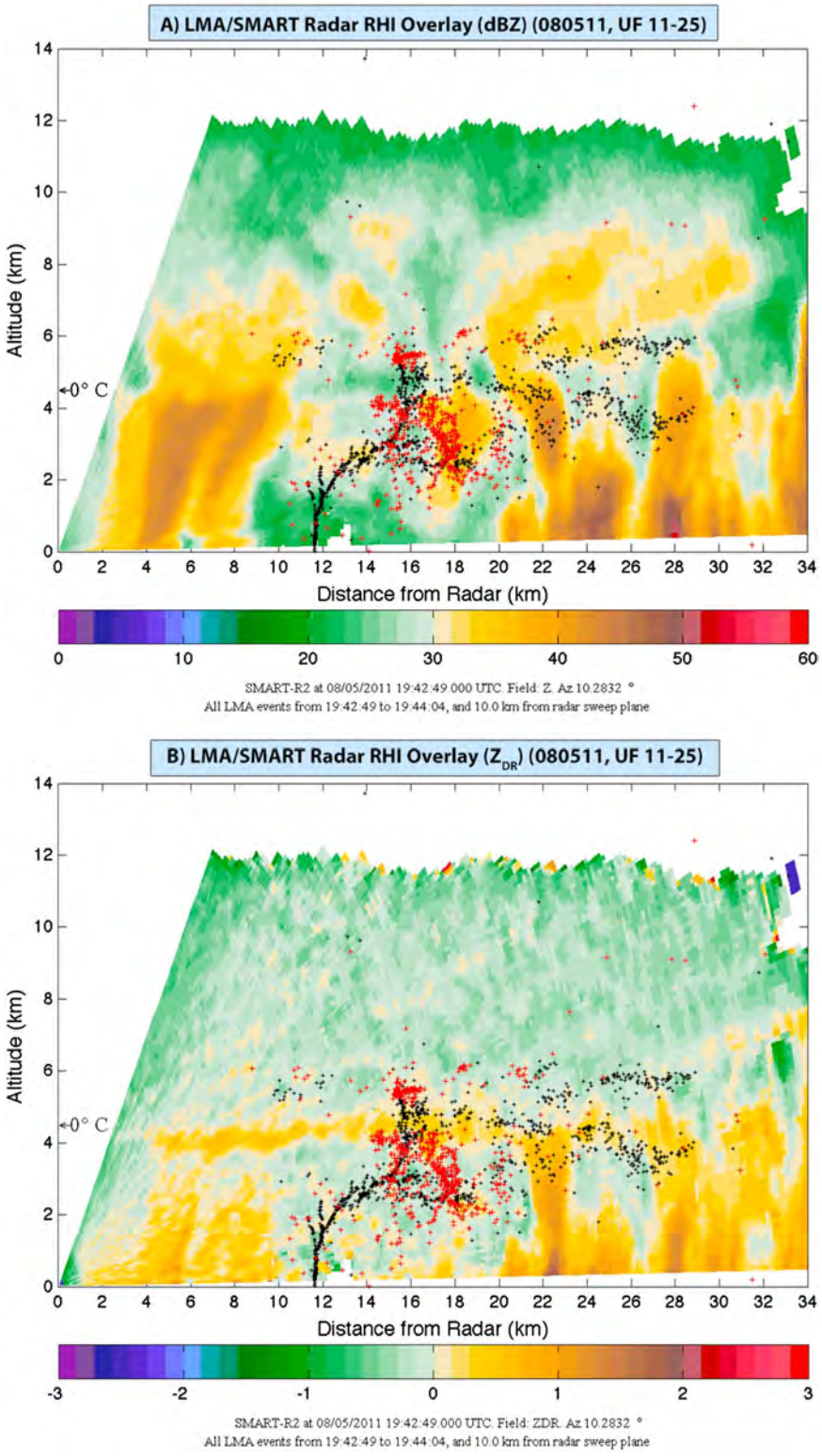

Figure 12. Modified RHI scans taken by the SMART radar at the time of flash UF 11-25 on 5 August 2011. (a) Filtered radar reflectivity (dBZ) with northing projection of LMA IS source locations overlaid. (b) Filtered and bias-corrected differential radar reflectivity factor (dB) with northing projection of LMA IS source locations overlaid. Projected LMA sources within 10 km of the RHI plane are plotted as black (red) crosses for source locations to the east (west) of the plane.

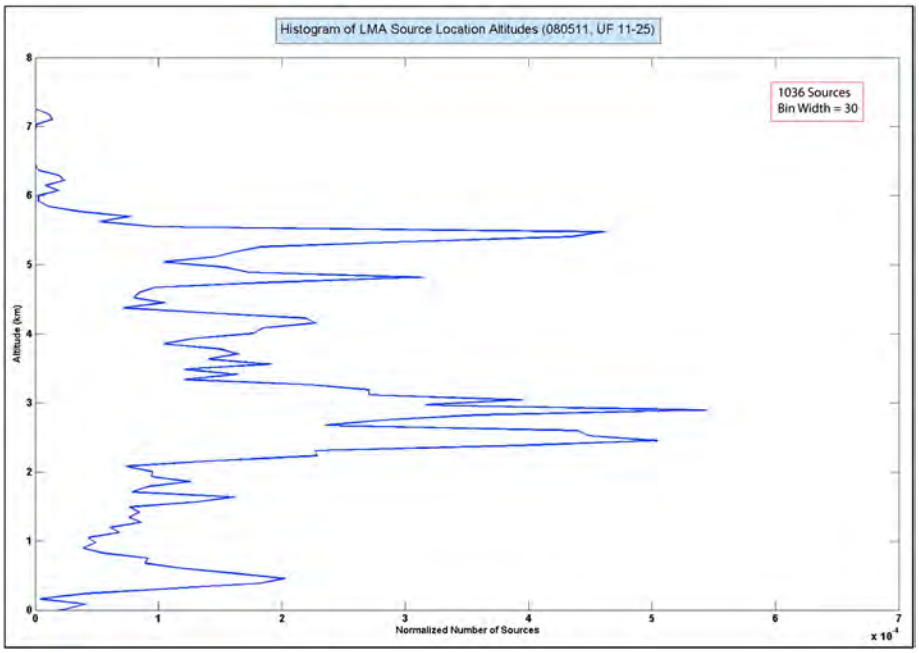

Figure 13. Histogram (bin size equal to 30 sources) of the altitude distribution of LMA IS sources of flash UF 11-25 on 5 August 2011.

process, and 282 ms before the first return stroke of flash UF 11-25. While the LMA sources for this flash are not shown in Figure 10 and are out of the plane of the radar RHI scan, the LMA sources indicate that the natural flash likely terminated 5–7 km to the northwest of the launching facility. While the removal of negative cloud charge due to the natural flash did not prevent the UF 11-25 dart leader/return stroke sequence from later traversing the path of the IS to ground, the natural flash may, in fact, have influenced the abnormally long time duration (about 400 ms) between the end of the IS and the UF 11-25 return stroke, a time period typically some tens of milliseconds in duration [e.g., *Rakov and Uman*, 2003]. Arguably, the wire-triggering process served to "trigger" the natural flash after the IS and before the triggered stroke. The low natural flash rate within 10 km of the launching facility observed via LMA data (five natural cloud-to-ground lightning discharges in the 10 min period preceding flash UF 11-25 and zero natural discharges in the 10 min period following flash UF 11-25) supports the argument.

[18] The distribution of LMA source altitudes during the IS of flash UF 11-25 is reproduced in Figure 13 from *Hill et al.* [2012a, 2012b]. The histogram includes a total of 1036 sources plotted with bin width of 30 sources. The features of the histogram of flash UF 11-25 are somewhat more complex than that of flash UF 11-14 due to the more extensive electrical breakdown that occurred at different altitudes.

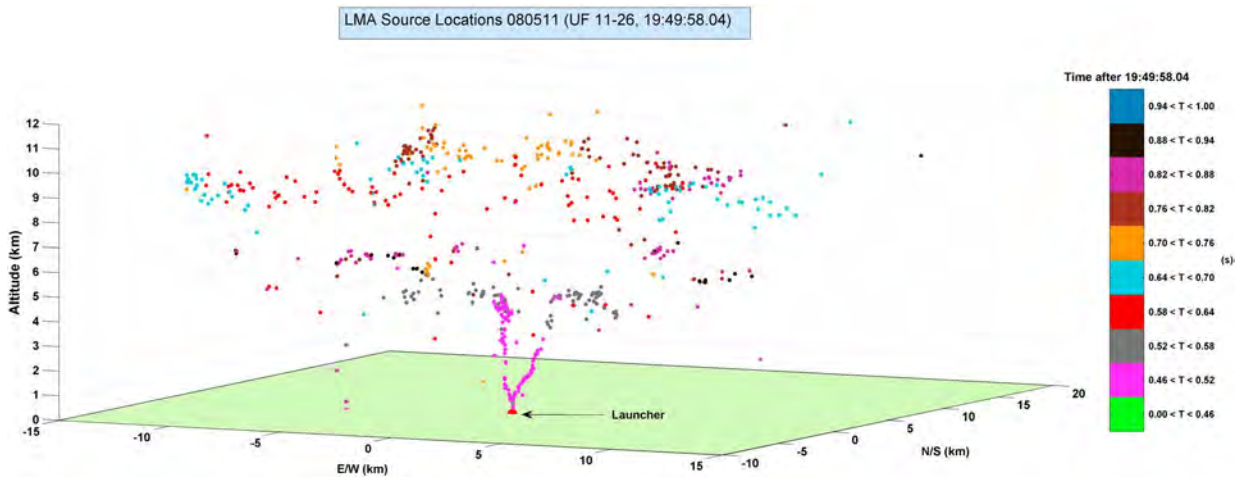

Figure 14. Three-dimensional plot of the LMA source locations for IS period of flash UF 11-26 on 5 August 2011. The sources span a total of 1 s beginning at 19:49:58.04 (UT). All LMA sources corresponding to precursor current pulses are colored in bright green and occupy the initial 460 ms of the displayed time window. LMA sources during the remainder of the IS process are color coded according to the key at right in 60 ms bins.

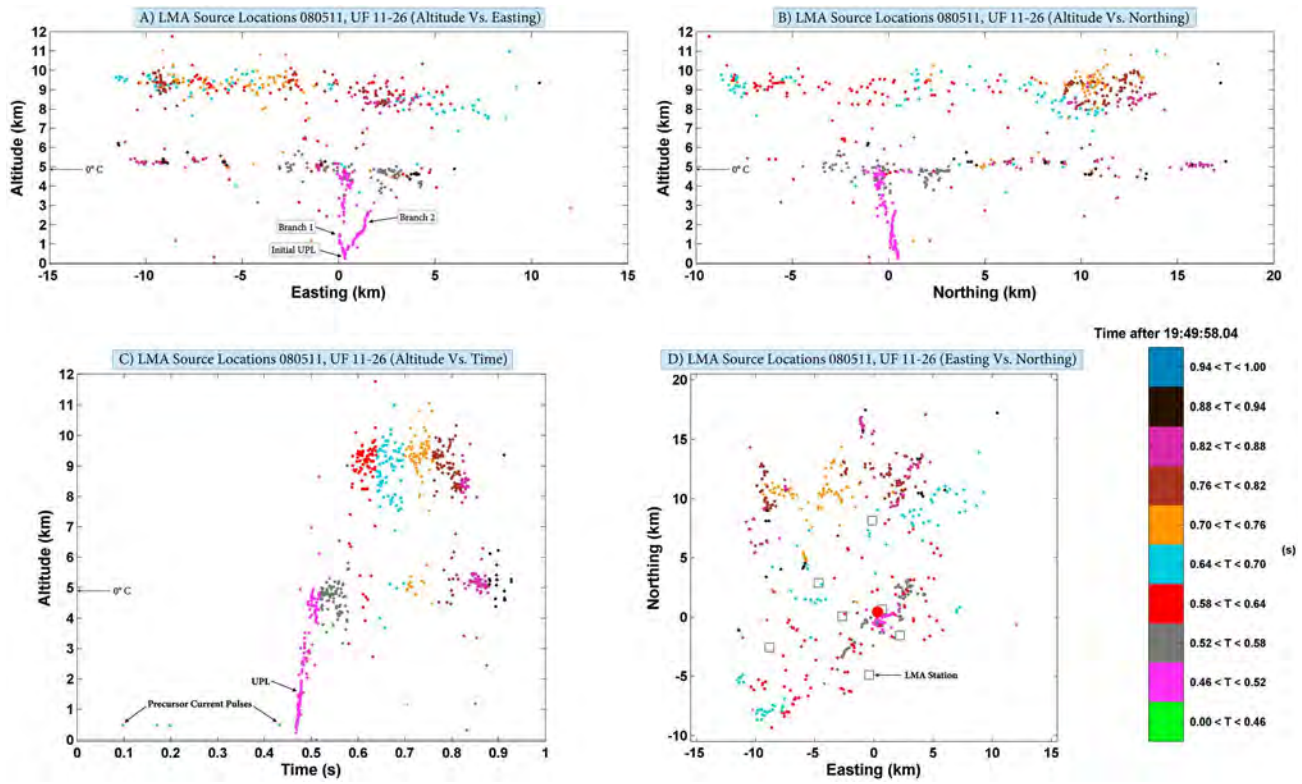

Figure 15. Four projection views of the LMA source locations for the IS period flash UF 11-26, including the intracloud discharge, on 5 August 2011. (a) An easting versus altitude plot (view looking due north), (b) a northing versus altitude plot (view looking due west), (c) an altitude versus time plot, and (d) an easting versus northing plot (plan view, launching facility annotated by large red circle). The sources span 4 s in time beginning at 19:49:58.04 (UT) and are color coded according to the convention of Figure 13. The initial UPL and two IS branches are labeled with increasing initiation time. The initiation altitudes of the two IS branches were 580 and 710 m, respectively.

The large number of sources below 2 km are from the initial UPL, branches 1 and 3 and the initial portion of branch 2. The histogram peaks around 3 km altitude are mostly due to the IS branches (branches 2, 5, and 6) that traveled to the north within the plane of the SMART radar RHI scan. There is also some contribution to the histogram peaks around 3 km from the western IS branches that occurred later in the IS process, and likely initiated the natural cloud-to-ground discharge 5–7 km northwest of the launching facility. The dominant histogram peaks between 5 and 6 km are from the IS branches that propagated along and above the 0°C level following the initial progression in the 3 km altitude range.

[19] As discussed above, many precursor current pulses were measured on the ascending triggering wire for flash UF 11-25, in large part due to the relatively long duration, about 4.4 s, between the rocket launch and the initiation of the UPL. The 33 precursor pulses located by both the LMA and by the ICLRT dE/dt (wideband, a few KHz to about 20 MHz) TOA network can be used to evaluate the accuracy of the ICLRT LMA system for low-altitude sources, treating the dE/dt TOA source locations as ground truth, that is, as accurate to within meters (see *Hill et al.* [2012a] for a discussion of dE/dt TOA accuracy). For flash UF 11-25, the closest LMA station to the launching facility was 2771 m east-southeast of the launcher (Table 1 and Figure 5d). For altitudes from 160 to 360 m determined by dE/dt TOA locations, the LMA overestimated the height of the source by an average of about 81 m. For dE/dt source altitudes between 375 and 455 m, the LMA overestimated the altitude location of the source by an average of only 34 m. From *Thomas et al.* [2004], the LMA altitude source uncertainty is given by equation 1

$$\Delta z = c\Delta t\left(\frac{d+r}{z}\right) \tag{1}$$

where d is the horizontal distance from the source to the closest measurement station, r is the radial distance from the source to the closest measurement station, and z is the source altitude. With the closest operating LMA station being at about 2.7 km, expected altitude errors are about 100 m for sources at 500 m altitude (for non noise-contaminated solutions), indicating that the small-area ICLRT LMA system is performing perhaps better than expected for low-altitude sources. In general, the LMA overestimated the easting coordinate of the precursor pulses by less than 25 m, with a gradually decreasing error with increasing height of the triggering wire. The easting source locations of the two TOA systems agreed to within 5 m for seven pulses. The LMA tended to overestimate the northing coordinate of the precursor sources by less than 20 m when the triggering wire was less than 350 m in altitude, although for 11 pulses, the locations of

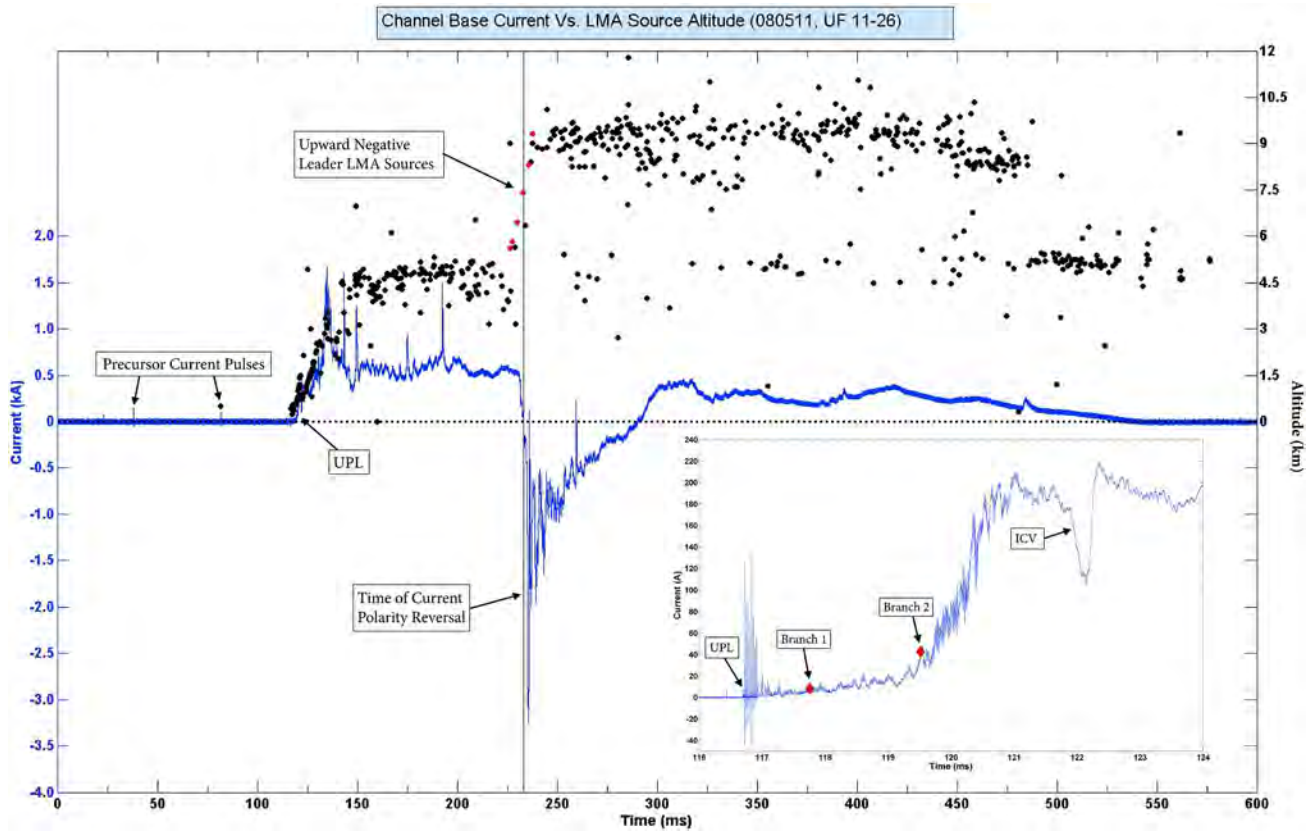

Figure 16. LMA source altitude locations (black points) for the IS period of flash UF 11-26, including the intracloud discharge, on 5 August 2011 overlaid on a 600 ms window of the low channel-base current measurement. The final 120 ms of the wire ascent and the full 433 ms duration of the UPL/ICC are shown. Sources are annotated corresponding to precursor current pulses. The time of the current polarity reversal measured at ground is annotated by a dotted vertical line. LMA sources corresponding to the upward-negative leader between the inferred main negative charge region and the lower portion of the upper positive charge region are shown in red color. The baseline current level is marked with a dotted horizontal line for reference. The inset at upper left shows an 8 ms window of the very low channel-base current waveform around the times of the UPL initiation, two IS branches, and the ICV. Red diamonds superimposed on the current waveform indicate the times of the two IS branches identified in Figure 15.

the two systems agreed to within 5 m. From 350 to 450 m in altitude, the LMA tended to underestimate the precursor source locations in the northing direction by less than 15 m, but for seven pulses, the locations of the two systems agreed to within 5 m. The accuracies of the LMA easting and northing source coordinates were not strong functions of altitude, as expected [e.g., *Thomas et al*., 2004].

3.3. Flash UF 11-26

[20] As noted earlier, triggered lightning discharges in Florida normally transport negative charge to ground via the IS process and any subsequent dart leader/return stroke sequences. Flashes UF 11-24 and UF 11-25 are examples of normal polarity-triggered lightning discharges, each containing an IS followed by one leader/return stroke sequence. Occasionally (statistics are found in section 4), triggered lightning current measured at the channel base undergoes a polarity reversal in its usual current indicating the lowering of positive charge to ground. Positive charge regions are reported to be present in typical thunderstorms both below and above the primary negative charge region, that is, above about 8 km and below about 6 km [e.g., *Marshall and Rust*, 1991; *Bringi et al*., 1997]; *Yoshida et al.* [2012] described a flash triggered at the ICLRT in 2009 (flash UF 09-30) in which the IS first lowered negative charge, then positive charge. *Yoshida et al.* [2012] used a 2-D VHF interferometer to infer the activity of a series of in-cloud leaders that were not initially connected to the IS channel but that subsequently led to the connection of an "upper level positive charge region" with the IS channel to ground. Further details are found in the section 4 of this paper. *Jerauld et al.* [2004] presented data for a two-stroke triggered flash in Florida whose first stroke lowered the expected negative charge following a negative IS while the second stroke unexpectedly lowered positive charge. The location of the charge source for the positive stroke could not be determined.

[21] Flash UF 11-26 first lowered negative charge to ground via the initial portion of the IS and then apparently induced a more or less natural-appearing bi-level intracloud discharge (as inferred from LMA data) via an upward-propagating negatively charged leader apparently between the main negative cloud charge region and the primary positive charge region above it. The intracloud discharge led to the lowering of positive charge through the IS channel, causing

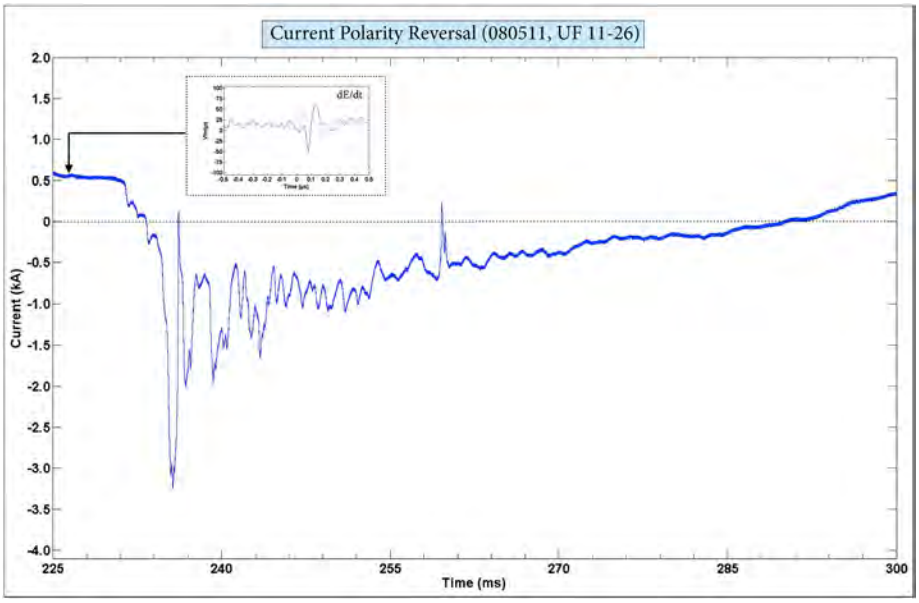

Figure 17. A 75 ms window of the channel-base current waveform (low measurement) shown in Figure 16 from 225 to 300 ms during the current polarity reversal of flash UF 11-26. The inset shows a 1 μs window around a dE/dt pulse corresponding to the initial LMA source of the upward-negative leader. The arrow indicates the time of the dE/dt pulse relative to the current waveform. The current baseline level is annotated with a dotted horizontal line for reference.

a current polarity reversal of about 57 ms duration to be observed at ground. Flash UF 11-26 produced no dart leader/return stroke sequences following the IS and intracloud discharge. Typical natural intracloud lightning flashes have previously been studied with LMA systems [e.g., *Thomas et al*., 2001; *Behnke et al*., 2005] and with 2-D interferometric systems [e.g., *Shao and Krehbiel*, 1996]. The data presented in this section provide strong evidence that the process of triggering lightning with a grounded wire can directly induce a normal polarity, bi-level intracloud discharge between the primary negative and upper positive cloud charge regions. LMA data indicate that there were zero natural cloud-to-ground or intracloud flashes within a 10 km radius of the launching facility in the 7 min periods before and after flash UF 11-26.

[22] Flash UF 11-26 was triggered at 19:49:58 (UT) on 5 August 2011 with a quasistatic electric field at ground of +5.6 kV/m. UF 11-26 was triggered about 7 min after flash UF 11-25 and 17 min after flash UF 11-24. At the time of the rocket launch, the reflectivity observed at an altitude of 600 m over the ICLRT by the Jacksonville WSR-88D had decreased to below 30 dBZ (Figure 1i). From the still image shown in Figure 3c, the conditions at ground level had continued to clear following flash UF 11-25. A 3-D plot of the LMA source locations for flash UF 11-26 is shown in Figure 14. In Figure 15, four projection views of the LMA source locations obtained during UF 11-26 are shown. Similar to the previous two cases, LMA sources associated with precursor current pulses are colored bright green, and sources during the UPL/ ICC are color coded in 60 ms bins according to the keys in Figures 14 and 15. The LMA detected only four precursor current pulses during the wire ascent, though many precursor current pulses were measured at ground (Figure 15c). The sustained UPL initiated at an altitude of about 177 m. The UPL depicted in Figure 15a propagated upward for about 2.5 ms at an average speed of 3.8×10^4 m/s before branching at an altitude of about 580 m. The initial IS branch (branch 1) propagated to the west, and 2.6 ms later, LMA sources show that a second IS branch (branch 2) initiated at an altitude of about 710 m and propagated towards the east. It is likely that branch 2 actually initiated at the same altitude as branch 1, though there is a gap in the LMA sources between the initiation points of branches 1 and 2 (the gap is not clearly visible at the spatial scales of Figures 14 and 15). The triggering wire exploded when the two IS branches reached about 750 m in altitude, about 5.2 ms following the initiation of the sustained UPL. The two IS channels then propagated generally upward and at an altitude of about 4.5 km, were separated laterally by about 2 km before turning horizontal near the 0 ° C level. Branch 1 traversed a total distance of about 2.8 km at an average speed of 1.8×10^4 m/s, and branch 2 propagated for about 4.1 km at an average speed of 4.7×10^4 m/s. Additional details are found in *Hill et al*. [2012b].

[23] In Figure 16, a 600 ms waveform of the measured low channel-base current and the altitude versus time projection of the LMA source locations (Figure 15c) are plotted. The current waveform was plotted using the low measurement since the UPL/ICC background current level was above the saturation point of the very low measurement and the UPL/ ICC contained many superimposed pulses with amplitudes greater than 1 kA. The current waveform shows the final 120 ms of the rocket ascent and the full 433 ms duration of the UPL/ICC process. About 114 ms after the initiation of the UPL, the channel-base current, which initially exhibited a polarity indicative of negative charge transport to ground, decreased sharply towards zero and subsequently changed polarity in a time span of about 2 ms. The time of the current polarity reversal is annotated in Figure 16 with a vertical line, and the baseline current level is shown with a dotted horizontal line. About 7 ms prior to the change in current

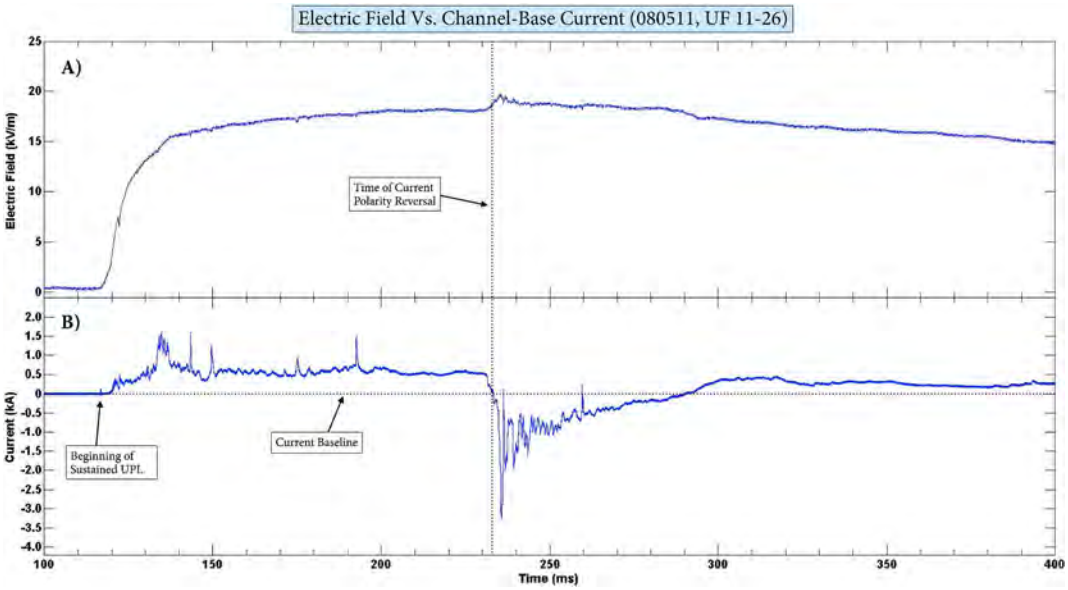

Figure 18. Electric field and channel-base current waveforms of flash UF 11-26. (a) A 300 ms waveform of the electric field measured by an antenna located 184 m from the lightning channel base and (b) a 300 ms waveform of the low channel-base current including the polarity reversal. The time scale corresponds to times from 100 to 400 ms in Figure 16. The time of the current polarity reversal is annotated with a dotted vertical line. Note the prominent hump in the electric field that begins in conjunction with the initial decrease of the channel-base current towards zero and about 5 ms prior to the current polarity reversal.

polarity, an upward-negative leader, characteristic of typical naturally occurring bi-level intracloud discharges, initiated at an altitude of about 5.6 km. The negative leader propagated from an altitude of 5.6 km to about 9.3 km in a time of 11 ms. The LMA leader sources are shown in red color in Figure 16, and their relatively high-source powers strongly suggest that they are of negative polarity. The upward-negative leader source powers recorded by the LMA ranged from 4–16 dBW, generally 1 to 2 orders of magnitude stronger than the preceding VHF sources recorded during the IS and associated with the extension of positively charged leaders. The upward-negative leader initiated about 3.5 km to the southwest of the launching facility and traversed a total distance of about 4.5 km with an average speed of about 4.1×10^5 m/s. Without accounting for channel tortuosity, the leader propagated at an angle from the vertical of about 18° at an azimuth of about 109° (southeast). The leader initiated widespread negative breakdown within the inferred upper positive charge region for about 270 ms following its 11 ms upward propagation period. The negative breakdown covered a lateral area of about 20 × 23 km and ranged in altitude from about 8 km to about 10 km. Positive breakdown at an altitude near 5 km, eventually covering a lateral area of about 18 × 25 km, occurred simultaneously with the higher-altitude negative breakdown. Individual channels in the intracloud discharge were poorly resolved at both altitude ranges, likely a result of the presence of many simultaneous channels and the 80 µs acquisition window per LMA source location (e.g., compare the branch detail of the intracloud channels in Figure 5 for flash UF 11-24 with the lack of branch detail in the case of flash UF 11-26). An 8 ms segment of the very low channel-base current waveform around the initiation times of the UPL and the two IS branches is plotted in the inset of Figure 16 at the bottom right. The times of the two IS branches are annotated on the current waveform with red diamonds. The IS branches initiated with channel-base current amplitudes of 9 and 43 A, respectively. Flash UF 11-26 exhibited a clear ICV which, as stated previously, occurred about 5.2 ms following the initiation of the sustained UPL, and is annotated in the inset of Figure 16.

[24] In Figure 17, a 75 ms plot of the current polarity reversal is shown. The timescale of Figure 16 corresponds to 225–300 ms in Figure 16. About 4.8 ms prior to the initial drop in magnitude of the channel-base current, between 230 and 231 ms in Figure 17, a bipolar dE/dt pulse (~115 V/m/µs peak-to-peak) was recorded by all 10 dE/dt sensors on the ICLRT dE/dt network. The initial polarity of the pulse is indicative of the upward movement of negative charge. The pulse corresponds in time to the first LMA source location of the upward-negative leader shown in Figure 16. A 1 µs window surrounding the dE/dt pulse is shown in the inset of Figure 17 at the upper left, and the arrow shows where in time the pulse occurred relative to the channel-base current waveform. The TOA location of the pulse from the ICLRT dE/dt network was within 290 m of the LMA source location (about 280 m laterally and about 20 m in altitude). Given that the source was well outside the boundary of the dE/dt TOA network, the lateral location errors of the dE/dt TOA system are expected to be of the order of 100 m and the altitude location error of the order of 200 m. It is also worth noting that the initial LMA source location of the upward-negative leader occurred coincident with a small rise in the measured channel-base current (immediately following the location of the arrow in Figure 17). No additional dE/dt pulses clearly corresponding to the ascending LMA sources of the upward-negative leader were resolved. About 2.3 ms following the current polarity reversal, the current magnitude fell sharply to a level of about −3.2 kA. The current waveform during

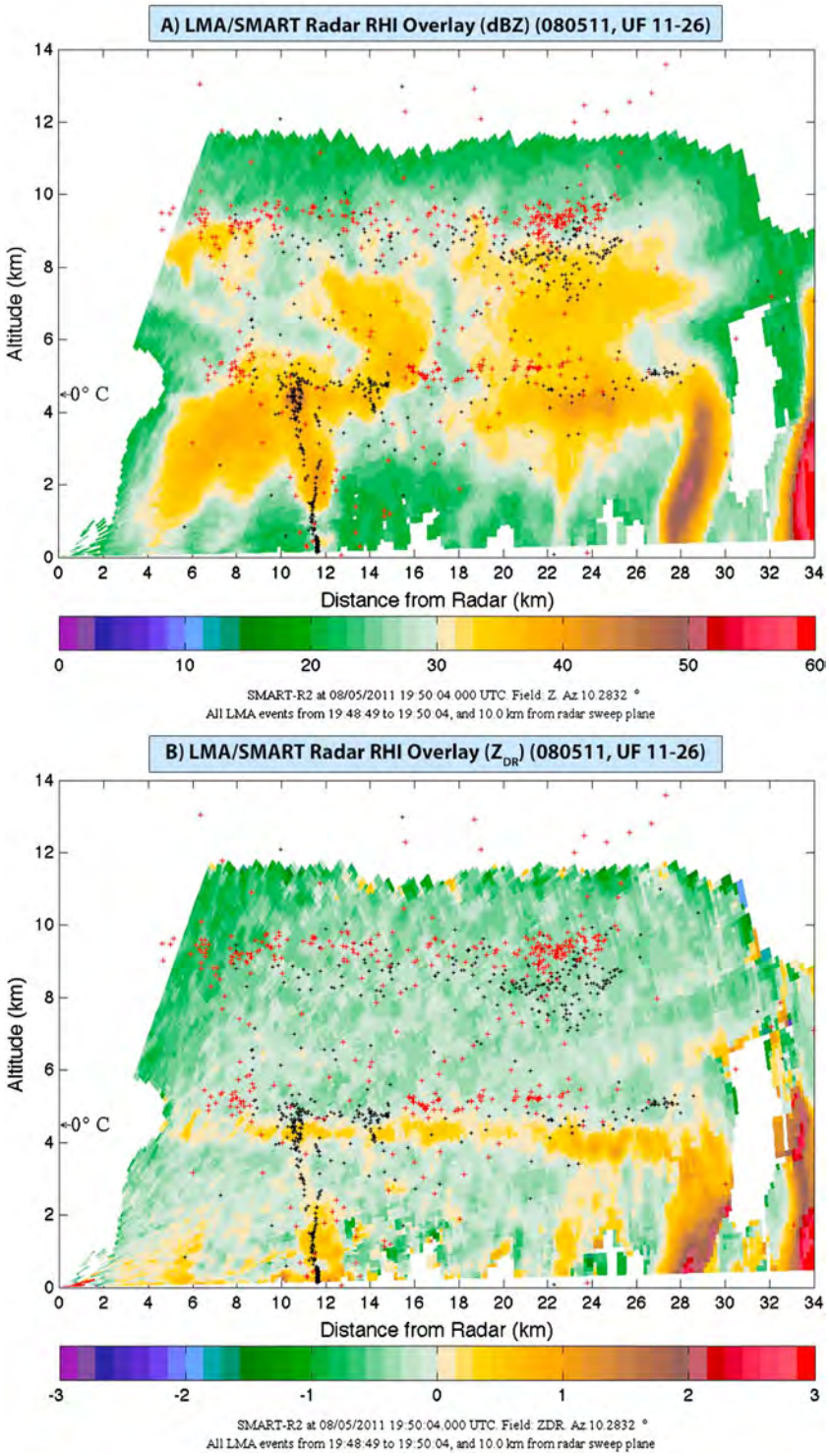

Figure 19. Modified RHI scans taken by the SMART radar at the time of flash UF 11-26 on 5 August 2011. (a) Filtered radar reflectivity (dBZ) with northing projection of LMA IS source locations overlaid. (b) Filtered and bias-corrected differential radar reflectivity factor (dB) with northing projection of LMA IS source locations overlaid. Projected LMA sources within 10 km of the RHI plane are plotted as black (red) crosses for source locations to the east (west) of the plane.

the full 56.8 ms duration of the polarity reversal is characterized by a continuous series of wide (~0.5–3 ms) pulses with amplitudes from several hundred amperes to several kiloamperes. The pulses are generally similar to negative ICC pulses [e.g., *Wang et al.*, 1999; *Miki et al.*, 2005] but, in this case, appear to be superimposed on an opposite-polarity background current that gradually tends back towards zero. It thus appears that both positive and negative charge sources were simultaneously available to the channel to ground. About 19 C of positive charge was transferred to ground during the current

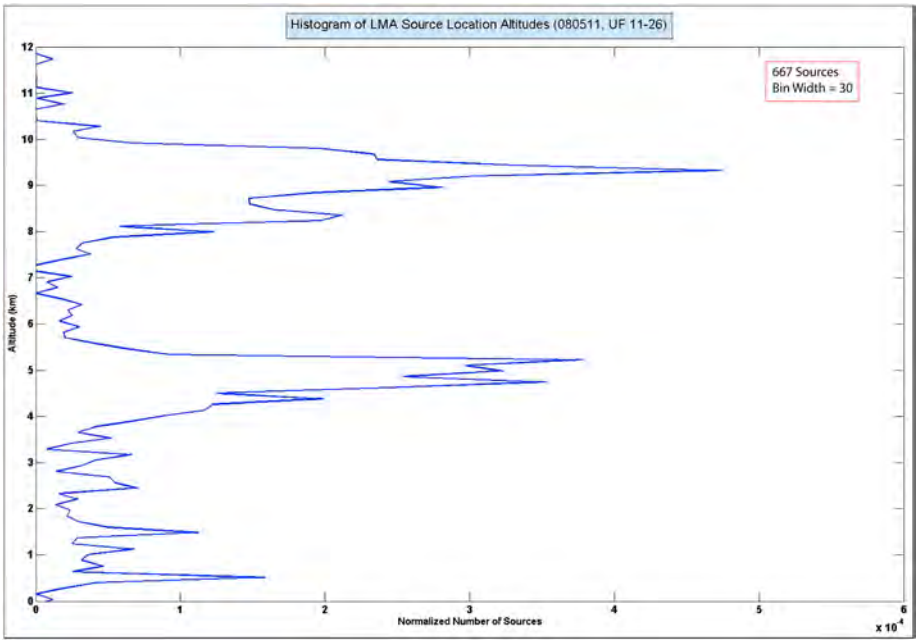

Figure 20. Histogram (bin size equal to 30 sources) of the altitude distribution of LMA sources of flash UF 11-26 on 5 August 2011.

polarity reversal, while the negative portion of the UPL/ICC transferred 120 C of charge to ground. The progression of the intracloud negative breakdown, as indicated by the LMA source locations, does not appear to be significantly altered when, after 56.8 ms of reverse current flow, the channel-base current reverted back to a polarity indicative of negative charge transport to ground.

[25] In Figure 18a, a 300 ms record of the time-varying electric field from the flat plate antenna 184 m from the launch facility is plotted corresponding to the time region from 100 to 400 ms in Figure 16. The channel-base current is plotted in Figure 18b for reference. Recall the electric field waveform was measured 184 m from the launching facility. The most interesting characteristic of the electric field waveform is the pronounced hump that is apparently associated with the initial deflection of the current towards zero, and starting about 5 ms prior to the current polarity reversal. The peak of the electric field hump occurred about 7.2 ms later, near the time of the next to last LMA source corresponding to the upward-negative leader at an altitude of about 8.3 km. The electric field change could well have started earlier in the waveform, closer to the time of the initiation of the upward-negative leader, and be simply unresolved due to lack of system sensitivity. *Yoshida et al*. [2012] show a very similar electric field waveform feature in their Figure 8f immediately prior to the current polarity reversal of flash UF 09-30.

[26] SMART radar RHI scans of dBZ and Z_{DR} at the time of flash UF 11-26 are shown in Figure 19. The northing projection of the LMA source locations (Figure 15b) during flash UF 11-26 is overlaid on each radar image. The precipitation at the ground surface was observed to have ended prior to the rocket launch that triggered flash UF 11-26 (see also the still image in Figure 3c). The RHI scans taken with the SMART radar show that the rocket and subsequent UPL rose through a tilted descending precipitation packet (PP) that was 2 km wide, on average, in the plane of the RHI and extended at least 1 km in the east–west direction, as determined by the 5° azimuthal RHI sector scan centered on the ICLRT. At the time of the rocket launch, the north–south width of the PP base was 600 m over the ICLRT and was found at an altitude of 500 m. A few hundred meters further east, however, the PP had already reached the ground surface. The PP formation may have been associated with remnants of the convective cell in the central part of the storm system but appeared as localized coalescence of raindrops just below the 0°C level. The vertical extent of the PP increased as larger drops fell faster than smaller drops, which led to an appreciable size-sorting signature in the Z_{DR}. Indeed, the lower portion of PP had areas where Z_{DR} values exceeded 2 dB while the upper portion had Z_{DR} values closer to 1 dB. Given the low reflectivity and high-Z_{DR} values in the base of the PP, it is likely that this region had low concentrations (less than one drop per cubic meter of air) of medium-to-large sized raindrops. When the IS channel turned horizontal near 4.5 km altitude, it propagated for some kilometers across the top of the PP and along the 0°C level (Figure 19a). Thus, the path of the initial UPL and the subsequent IS channel development were closely associated with precipitation boundaries.

[27] The majority of the LMA sources during the current polarity reversal at ground were located in a layer between 8 and 10 km in altitude and were associated with precipitation near the cores of dissipating convective cells to the north and southwest of the ICLRT. SMART radar reflectivity indicates that the anvil of the cloud system was inhomogeneous, with regions of reflectivity approaching 35 dBZ in the 8–10 km layer (Figure 19a). The LMA sources during the charge reversal suggest the negative breakdown occurred near the tops of these enhanced reflectivity regions. One of the enhanced reflectivity regions, observed between 5–8 km range and 8–9.5 km in altitude at 19:50 (UT), had Z_{DR} values that were negative on average. The surrounding regions, with lower radar reflectivity, had Z_{DR} values closer to zero.

Negative Z_{DR} aloft is often associated with ice crystals that become vertically aligned by strong vertical electric fields [e.g., *Hendry et al*., 1976]. It is noteworthy that projection of the LMA sources onto the plane of the RHI showed that the majority of the initial few LMA sources during the charge reversal fell within this region of mean negative Z_{DR}. While the narrow section sampled by the radar during this time did not include the dissipating cell to the southwest of the ICLRT (Figures 1 and 2) where the initial few LMA sources occurred, adjacent RHI scans suggest that this region of negative Z_{DR} did extend westward.

[28] Aspects of the cloud charge structure during flash UF 11-26 can be inferred from the altitude distribution of LMA source locations. Figure 20 shows a histogram (bin width of 30 source points) of the LMA source altitudes for 667 sources. The bimodal distribution of source altitudes together with the corresponding source powers measured by the LMA indicates a region of predominantly positive electrical breakdown spanning an altitude from about 4.0 to 5.5 km and a region of predominantly negative breakdown spanning in altitude from about 7.5 to 10.5 km. The electric fields are highest on the outer boundaries of the charge region so the exact relation between the LMA breakdown location and the charge sources before the intracloud discharge is not completely determinate. The unknown is how far and how thoroughly the discharges penetrate the charge regions. LMA images of natural lightning flashes in the 5 min period prior to flash UF 11-24 show that the top of the negative charge region likely occurred at 7.5–8 km altitude. In the 10 min period between flashes UF 11-24 and UF 11-25, the top of the negative charge region appears to have descended to 6–7 km, though the data set of flashes within 10 km of the launching facility was limited. If the trend continued as the storm decayed, it is reasonable that the top of the negative charge layer at the time of flash UF 11-26 was located at 5.5–6 km altitude. As previously noted, there were no natural flashes in the 7 min prior to flash UF 11-26 with which to directly compare the LMA data.

[29] The vertical structure of the electrical breakdown suggests that the upward-negative leader, which propagated from 5.6 to 9.3 km in altitude, connected the expected top of the negative charge region to the lower part of the upper positive charge region. In the process, a path was developed for some positive charge, about 19 C, to flow through the IS channel to ground.

4. Discussion

[30] The three triggered flashes documented here occurred within a transition zone [e.g., *Biggerstaff and Houze*, 1993] between convective areas of a dissipating multicell cloud system that propagated slowly westward over the launch facility during 5 August 2011. Each successive rocket launch occurred in gradually weakening precipitation at the ground, with the last launch (UF 11-26) occurring after rain had initially ceased at the launch facility. At higher altitudes, however, a tilted descending precipitation pulse was near the ICLRT at the time of the rocket launch, with the bottom of the precipitation pulse located about 500 m above the launch facility. A few hundred meters east, the precipitation pulse had already reached the surface. The lowest 1.5 km of the IS of flash 11-25 traveled along or near the boundary of a convective-scale rain shaft surrounded by much weaker precipitation. The lower portion of the IS of flash UF 11-24 traveled along a more subtle gradient in precipitation. It is possible that the descending precipitation in these pulses was associated with locally enhanced electric fields that may have aided breakdown along the lower altitude portion of the IS. The relatively long quasi-horizontal IS path of flash UF 11-25 below the 0°C level was also likely affected by the spatial distribution of enhanced precipitation below the melting layer.

[31] Farther aloft, the IS in all three flashes exhibited an extensive horizontal path along the top of the Z_{DR}-indicated melting layer. As exhibited by flash UF 11-24, the IS path can change abruptly from mostly vertical to mostly horizontal at this altitude. Above the top of the melting layer, all three flashes behaved differently. UF 11-24 branched near the transition between water-coated and frozen hydrometeors at the base of an upper level convective turret. A portion of the IS of flash UF 11-25 traveled to 6 km altitude before turning horizontal with LMA sources having a tendency to cluster near the transitions between positive and negative Z_{DR}. In contrast, flash UF 11-26 induced a bipolar intracloud discharge with LMA sources extending to about 10 km altitude. Most of those sources occurred along the top of the enhanced (> 30 dBZ) radar reflectivity regions that extended to 10 km altitude.

[32] The fact that the IS channels turn horizontal in the altitude range of the 0°C level [see also *Yoshida et al*., 2010; *Hill et al*., 2012b] indicates a preferred path for propagation either because of high-electric fields [e.g., *Coleman et al*., 2003, 2008] and concentrated charge or that characteristics of the particular hydrometeors present in that range allow for a lowered breakdown electric field, or perhaps a combination thereof. For example, *Shepherd et al*. [1996], from balloon measurements, found positive charge near the melting level in stratiform clouds with less concentrated negative charge below in the presence of a radar bright band that marked the melting level. A UPL would be attracted to such a negative charge region and forced to remain below the higher positive charge region by its downward-pointing electric field. Past studies have reported charge near the 0°C level of stratiform or collapsing convective clouds [e.g., *Marshall and Lin*, 1992; *Stolzenburg et al*., 1998], with positive charge being perhaps the most commonly found concentrated charge. *Shepherd et al*. [1996] and others have associated the layers of charge near the 0°C level with the melting process, as evidenced by the presence of a radar bright band. It is not evident how well the charge structures in the vicinity of the 0°C level reported in the previous literature correlate to the stratiform-like conditions present during the triggered lightning flashes described here, which occurred in a low-altitude, coastal environment.

[33] The relationship between LMA source locations and precipitation structure strongly suggests that the propagation of the IS of these triggered flashes was affected by hydrometeor distributions. What is less clear, however, is whether the radar structure, like the top of the melting layer, simply delineates charge regions within the cloud or, like the descending precipitation packets, may actively contribute to local enhancements in electric fields or lowering of the breakdown field by hydrometeors that aid the propagation of the IS.

[34] *Hill et al*. [2012b] measured the IS branching and speed characteristics of nine triggered flashes, including UF 11-24, UF 11-25, and UF 11-26, but presented no radar data.

The average UPL/ICC charge transfer and duration for the nine flashes was 104 C (median of 120 C) and 578 ms (median of 597 ms), respectively. Flashes UF 11-24 and UF 11-25 had measured UPL/ICC charge transfers of 46 C and 28 C, respectively, both significantly less than the average charge transfer for the nine flash data set. The UPL/ICC durations of flashes UF 11-24 and UF 11-25 were 428 ms and 404 ms, also somewhat less than the average duration for the full data set. The physical significance, if any, of the above observations is not evident considering the geometries of the IS processes of flashes UF 11-24 and UF 11-25, as determined from the LMA source locations, were not abnormal with respect to the number and extent of horizontal IS branches. Flash UF 11-26 exhibited channel-base current characteristics during the IS period that were more representative of the full data set, excluding the observed polarity reversal, with UPL/ICC charge transfer of 120 C (negative charge only) and duration of 433 ms.

[35] The average 3-D speed of the UPL channel prior to branching for the three flashes discussed here was 6.7×10^4 m/s (8.4×10^4, 7.9×10^4, and 3.8×10^4 m/s for flashes UF 11-24, UF 11-25, and UF 11-26, respectively) similar to the average speed of 8.7×10^4 m/s for all nine flashes. As discussed in *Hill et al*. [2012b], the average UPL speed of the three flashes in this study was slower than the 3-D UPL speeds of 2.2×10^6 and 3.3×10^6 m/s calculated by *Yoshida et al*. [2010] for two flashes, and in much better agreement with the 2-D UPL speeds of 5.6×10^4 m/s given by *Biagi et al*. [2009] and 1.0×10^5 m/s given by *Jiang et al*. [2011], the first two studies being conducted at the ICLRT and the later *Jiang et al*. [2011] study in China. The speed of the UPL channel prior to branching for flash UF 11-24 was a factor of about 2 to 4 larger than those of the four subsequent IS branches, all of which initiated above 5 km altitude. For flash UF 11-25, the speed of the UPL channel prior to branching was comparable to the initial three IS branches, all of which initiated at altitudes below 1.5 km, and a factor of 2 to 3 larger than the subsequent three IS branches, which initiated at altitudes above 2 km. The first IS branches of flashes UF 11-25 and UF 11-26 initiated at lower altitudes (750 and 580 m, respectively) than the average for the full data set of about 2.4 km (median of 1.6 km), while the initial IS branch of flash UF 11-24 occurred at an altitude of 5.2 km and as stated previously, was preceded by a 12.6 km, mostly horizontal, unbranched UPL channel.

[36] Current polarity reversals during the UPL/ICC periods of triggered lightning flashes have been rarely observed at the ICLRT, having occurred in only 2 out of a total of 77 (~2.6 %) events from 2008 to 2012. The first case occurred in 2009 and is documented in *Yoshida et al*. [2012]. The second is flash UF 11-26. The current polarity reversal measured at ground in *Yoshida et al*. [2012] was shorter in duration (39 ms versus 56.8 ms for flash UF 11-26) but transferred more positive charge (29 C versus 19 C for UF 11-26) and exhibited a higher-magnitude peak current during the reversal period (−5.5 kA versus −3.2 kA for UF 11-26). *Yoshida et al*. [2012] used a broadband interferometer to infer the presence of a connecting leader between the main negative and upper positive charge regions that initiated 7.6 ms prior to the observed current polarity reversal, but they do not provide geometrical characteristics of the leader. Unlike UF 11-26, which had no subsequent return strokes, the event discussed in *Yoshida et al*. [2012] had one dart leader/subsequent return stroke sequence with peak stroke current of 29.6 kA following a 140 ms zero-current interval at the cessation of the IS. The time duration (11 ms) and average 3-D speed (4.1×10^5 m/s) of the intracloud-flash-initiating upward-negative leader recorded by the LMA for flash UF 11-26 are in good agreement with statistics reported by *Shao and Krehbiel* [1996], who used a narrowband interferometer to determine upward-negative leader durations of 10–20 ms and propagation speeds of 1.5 to 3×10^5 m/s for bi-level intracloud flashes in central Florida, and with statistics reported by *Behnke et al*. [2005], who used LMA sources to calculate the median initial upward-negative leader speed to be 1.6×10^5 m/s for 24 intracloud flashes in New Mexico and Kansas. The upward-negative leader in this Florida study appeared to have initiated at an altitude of about 5.6 km, several kilometers lower than those reported by *Shao and Krehbiel* [1996] and *Behnke et al*. [2005] for naturally occurring bi-level intracloud discharges, both studies reporting initial altitudes of about 7–8 km. The LMA sources during the time of the current polarity reversal were predominantly in the 8–10 km layer, where positive charge would likely be found. Projection of the first 12 source locations into the radar RHI plane indicated that all these sources occurred near the negative Z_{DR} region in the upper left portion of the RHI (Figure 19b). *Seliga et al*. [1983] and *Scott et al*. [2001] showed that negative Z_{DR} aloft can be associated with alignment of ice crystals by strong electric fields. *Lund et al*. [2009] found that upper level negative Z_{DR} regions can be preferred locations for naturally occurring flash initiation. Thus, it appears that the upward-propagating negative leader first tapped into strong electric fields in the cell to the southwest before spreading more horizontally along the tops of the upper level enhanced reflectivity regions.

[37] We suggest that the horizontally propagating, positively charged IS channels that propagate along the contour of the 0°C level could well have deposited positive charge (or neutralized negative charge) below the main negative charge region and hence enhanced the electric field at the bottom of the main negative charge region, thereby increasing the probability that a downward-propagating negative leader could initiate. This scenario evidently occurred 119 ms following the IS of flash UF 11-25, when a negative leader descended from an apparent altitude of 2.5–4 km and resulted in a nearby cloud-to-ground discharge. It also follows that addition of positive charge below the main negative charge region should decrease the electric field at the top of the negative charge region, lessening the probability of an upward leader initiation between the top of the main negative charge region and the positive charge center above. However, in the case of flash UF 11-26, the propagating positive IS channels and their charge deposition appear to have provided suitable conditions at an altitude of 5.6 km for launching an upward-negative leader that initiated a more or less natural bi-level intracloud discharge.

[38] **Acknowledgments.** This research was primarily funded by the DARPA NIMBUS program with additional support from NASA. M. Biggerstaff was partially supported by National Science Foundation grant AGS-1063537. The authors would also like to thank G. Carrie, K. Thiem, T. Ngin, W. Gamerota, N. Brooks, A. Dunhoft, and J. Jordan for their assistance in the data collection effort.

References

Behnke, S. A., R. J. Thomas, P. R. Krehbiel, and W. Rison (2005), Initial leader velocities during intracloud lightning: Possible evidence for a runaway breakdown effect, *J. Geophys. Res.*, *110*, D10207, doi:10.1029/2004JD005312.

Biagi, C. J., D. M. Jordan, M. A. Uman, J. D. Hill, W. H. Beasley, and J. Howard (2009), High-speed video observations of rocket-and-wire initiated lightning, *Geophys. Res. Lett.*, *36*, L15801, doi:10.1029/2009GL038525.

Biagi, C. J., M. A. Uman, J. D. Hill, D. M. Jordan, and V. A. Rakov (2012), Transient current pulses in rocket-extended wires used to trigger lightning, *J. Geophys. Res.*, *117*, D07205, doi:10.1029/2011JD016161.

Biggerstaff, M. I., and R. A. Houze Jr. (1993), Kinematics and microphysics of the transition zone of the 10–11 June 1985 squall-line system, *J. Atmos. Sci.*, *50*, 3,091–3,110.

Biggerstaff, M. I., L. J. Wicker, J. Guynes, C. Ziegler, J. M. Straka, E. N. Rasmussen, A. Dogget IV, L. D. Carey, J. L. Schroeder, and C. Weiss (2005), The Shared Mobile Atmospheric Research And Teaching (SMART) Radar: A collaboration to enhance research and teaching, *Bull. Am. Meteorol. Soc.*, *86*, 1,263–1,274.

Bringi, V. N., K. Knupp, A. Detwiler, L. Liu, I. J. Caylor, and R. A. Black (1997), Evolution of a Florida thunderstorm during the convection and precipitation/electrification experiment: The case of 9 August 1991, *Mon. Weather Rev.*, *125*, 2,131–2,160.

Carey, L. D., and S. A. Rutledge (1996), A multiparameter radar case study of the microphysical and kinematic evolution of a lightning producing storm, *Meteorol. Atmos. Phys.*, *59*, 33–64.

Coleman, L. M., T. C. Marshall, M. Stolzenburg, T. Hamlin, P. R. Krehbiel, W. Rison, and R. J. Thomas (2003), Effects of charge and electrostatic potential on lightning propagation, *J. Geophys. Res.*, *108*, 4298, doi:10.1029/2002JD002718.

Coleman, L. M., M. Stolzenburg, T. C. Marshall, and M. Stanley (2008), Horizontal lightning propagation, preliminary breakdown, and electric potential in New Mexico thunderstorms, *J. Geophys. Res.*, *113*, D09208, doi:10.1029/2007JD009459.

Crum, T. D., and R. L. Alberty (1993), The WSR-88D and the WSR-88D Operational Support Facility, *Bull. Am. Meteorol. Soc.*, *74*, 1,669–1,687.

Edens, H. E., et al. (2012), VHF lightning mapping observations of a triggered lightning flash, *Geophys. Res. Lett.*, *39*, L19807, doi:10.1029/2012GL053666.

French, J. R., J. H. Helsdon, A. G. Detwiler, and P. L. Smith (1996), Microphysical and electrical evolution of a Florida thunderstorm: 1. Observations, *J. Geophys. Res.*, *101*(D14), 18,961–18,977.

Gremillion, M. S., and R. E. Orville (1999), Thunderstorm characteristics of cloud-to-ground lightning at the Kennedy Space Center, Florida: A study of lightning initiation signatures as indicated by the WSR-88D, *Wea. Forecasting*, *14*, 640–649.

Hansen, A. E., H. E. Fuelberg, and K. E. Pickering (2010), Vertical distributions of lightning sources and flashes over Kennedy Space Center, Florida, *J. Geophys. Res.*, *115*, D14203, doi:10.1029/2009JD013143.

Harris, G. N., Jr., K. P. Bowman, and D.-B. Shin (2000), Comparison of freezing-level altitudes from the NCEP reanalysis with TRMM Precipitation Radar brightband data, *J. Climate*, *13*, 4,137–4,148.

Hendry, A., G. C. McCormick, and B. L. Barge (1976), The degree of common orientation of hydrometeors observed by polarization diversity radars, *J. Appl. Meteorol.*, *15*, 633–640.

Hill, J. D., M. A. Uman, D. M. Jordan, J. R. Dwyer, and H. Rassoul (2012a), "Chaotic" dart leaders in triggered lightning: Electric fields, X-rays, and source locations, *J. Geophys. Res.*, *117*, D03118, doi:10.1029/2011JD016737.

Hill, J. D., J. Pilkey, M. A. Uman, D. M. Jordan, W. Rison, and P. R. Krehbiel (2012b), Geometrical and electrical characteristics of the initial stage in Florida triggered lightning, *Geophys. Res. Lett.*, *39*, L09807, doi:10.1029/2012GL051932.

Jerauld, J., M. A. Uman, V. A. Rakov, K. J. Rambo, and D. M. Jordan (2004), A triggered lightning flash containing both negative and positive strokes, *Geophys. Res. Lett.*, *31*, L08,104, doi:10.1029/2004GL019457.

Jiang, R., X. Qie, C. Wang, and J. Yang (2011), Step-like characteristics of an upward positive leader in triggered lightning, *Lightning* (*APL*), *2011 7th Asia-Pacific International Conference on*, vol., no., pp.614–617, 1–4 Nov. 2011, doi:10.1109/APL.2011.6110200.

Krehbiel, P. R. (1986), The Earth's electrical environment, in *The Electrical Structure of Thunderstorms*, pp. 90–113, National Academy Press., Washington, DC.

Krehbiel, P. R., R. J. Thomas, W. Rison, T. Hamlin, J. Harlin, and M. Davis (2000), Lightning mapping observations in central Oklahoma, *Eos. Trans. AGU*, *81*(3), 21–25.

Lalande, P., A. Bondiou-Clergerie, P. Laroche, A. Eybert-Berard, J.-P. Berlandis, B. Bador, A. Bonamy, M. A. Uman, and V. A. Rakov (1998), Leader properties determined with triggered lightning techniques, *J. Geophys. Res.*, *103*(D12), 14,109–14,115, doi:10.1029/97JD02492.

Lund, N. R., D. R. MacGorman, T. J. Schuur, M. I. Biggerstaff, and W. D. Rust (2009), Relationships between lightning location and polarimetric radar signatures in a small mesoscale convective system, *Mon. Weather Rev.*, *137*, 4,151–4,170.

Marshall, T. C., and B. Lin (1992), Electricity in dying thunderstorms, *J. Geophys. Res.*, *97*(D9), 9,913–9,918, doi:10.1029/92JD00463.

Marshall, T. C., and W. D. Rust (1991), Electric field soundings through thunderstorms, *J. Geophys. Res.*, *96*(D12), 22,297–22,306, doi:10.1029/91JD02486.

Miki, M., V. A. Rakov, T. Shindo, G. Diendorfer, M. Mair, F. Heidler, W. Zischank, M. A. Uman, R. Thottappillil, and D. Wang (2005), Initial stage in lightning initiated from tall objects and in rocket-triggered lightning, *J. Geophys. Res.*, *110*, D02109, doi:10.1029/2003JD004474.

Olsen, R. C., III, V. A. Rakov, D. M. Jordan, J. Jerauld, M. A. Uman, and K. J. Rambo (2006), Leader/return-stroke-like processes in the initial stage of rocket-triggered lightning, *J. Geophys. Res.*, *111*, D13202, doi:10.1029/2005JD006790.

Rakov, V. A., and M. A. Uman (2003), *Lightning: Physics and Effects*, Cambridge Univ. Press, Cambridge, United Kingdom.

Rakov, V. A., D. E. Crawford, V. Kodali, V. P. Idone, M. A. Uman, G. H. Schnetzer, and K. J. Rambo (2003), Cutoff and reestablishment of current in rocket-triggered lightning, *J. Geophys. Res.*, *108*(D23), 4747, doi:10.1029/2003JD003694.

Rison, W., R. J. Thomas, P. R. Krehbiel, T. Hamlin, and J. Harlin (1999), A GPS-based three-dimensional lightning mapping system: Initial observations in central New Mexico, *Geophys. Res. Lett.*, *26*, 3,573–3,576.

Scott, R. D., P. R. Krehbiel, and W. Rison (2001), The use of simultaneous horizontal and vertical transmissions for dual-polarization radar meteorological observations, *J. Atmos. Oceanic Technol.*, *18*, 629–648.

Seliga, T. A., K. Aydin, H. Direskeneli, and V. N. Bringi (1983), Possible evidence for strong vertical electric fields in thunderstorms from differential reflectivity measurements, *Proc. 21st AMS Conference on Radar Meteorology*, Edmonton, Sept. 19–23.

Shao, X. M., and P. R. Krehbiel (1996), The spatial and temporal development of intracloud lightning, *J. Geophys. Res.*, *101*(D21), 26,641–26,668, doi:10.1029/96JD01803.

Shepherd, T. R., W. D. Rust, and T. C. Marshall (1996), Electric fields and charges near 0°C in stratiform clouds, *Mon. Weather Rev.*, *124*, 919–938.

Stolzenburg, M., W. D. Rust, B. F. Smull, and T. C. Marshall (1998), Electrical structure in thunderstorm convective regions: 1. Mesoscale convective systems, *J. Geophys. Res.*, *103*(D12), 14,059–14,078, doi:10.1029/97JD03546.

Thomas, R. J., P. R. Krehbiel, W. Rison, T. Hamlin, J. Harlin, and D. Shown (2001), Observations of VHF source powers radiated by lightning, *Geophys. Res. Lett.*, *28*(1), 143–146, doi:10.1029/2000GL011464.

Thomas, R. J., P. R. Krehbiel, W. Rison, S. J. Hunyady, W. P. Winn, T. Hamlin, and J. Harlin (2004), Accuracy of the Lightning Mapping Array, *J. Geophys. Res.*, *109*, D14207, doi:10.1029/2004JD004549.

Wang, D., V. Rakov, M. Uman, M. Fernandez, K. Rambo, G. Schnetzer, and R. Fisher (1999), Characterization of the initial stage of negative rocket-triggered lightning, *J. Geophys. Res.*, *104*(D4), 4,213–4,222.

Willett, J. C., D. A. Davis, and P. Laroche (1999), An experimental study of positive leaders initiating rocket-triggered lightning, *Atmos. Res.*, *51*, 189–219.

Yoshida, S., C. J. Biagi, V. A. Rakov, J. D. Hill, M. V. Stapleton, D. M. Jordan, M. A. Uman, T. Morimoto, T. Ushio, and Z.-I. Kawasaki (2010), Three-dimensional imaging of upward positive leaders in triggered lightning using VHF broadband digital interferometers, *Geophys. Res. Lett.*, *37*, L05805, doi:10.1029/2009GL042065.

Yoshida, S., et al. (2012), The initial stage processes of rocket-and-wire triggered lightning as observed by VHF interferometry, *J. Geophys. Res.*, *117*, D09119, doi:10.1029/2012JD017657.

Zrnic, D. S., and A. V. Ryzhkov (1999), Polarimetry for weather surveillance radars, *Bull. Am. Meteorol. Soc.*, *80*, 389–406.